

AWARD NUMBER: W81XWH-14-1-0576

TITLE: Understanding and Targeting Tumor Microenvironment in Prostate Cancer to Inhibit Tumor Progression and Castration Resistance

PRINCIPAL INVESTIGATOR: Yaoqi Alan Wang

CONTRACTING ORGANIZATION: MD Anderson Cancer Center  
Houston, TX 77030

REPORT DATE: December 2017

TYPE OF REPORT: Final

PREPARED FOR: U.S. Army Medical Research and Materiel Command  
Fort Detrick, Maryland 21702-5012

DISTRIBUTION STATEMENT: Approved for Public Release;  
Distribution Unlimited

The views, opinions and/or findings contained in this report are those of the author(s) and should not be construed as an official Department of the Army position, policy or decision unless so designated by other documentation.

# REPORT DOCUMENTATION PAGE

Form Approved  
OMB No. 0704-0188

Public reporting burden for this collection of information is estimated to average 1 hour per response, including the time for reviewing instructions, searching existing data sources, gathering and maintaining the data needed, and completing and reviewing this collection of information. Send comments regarding this burden estimate or any other aspect of this collection of information, including suggestions for reducing this burden to Department of Defense, Washington Headquarters Services, Directorate for Information Operations and Reports (0704-0188), 1215 Jefferson Davis Highway, Suite 1204, Arlington, VA 22202-4302. Respondents should be aware that notwithstanding any other provision of law, no person shall be subject to any penalty for failing to comply with a collection of information if it does not display a currently valid OMB control number. **PLEASE DO NOT RETURN YOUR FORM TO THE ABOVE ADDRESS.**

<b>1. REPORT DATE</b> December 2017		<b>2. REPORT TYPE</b> Final		<b>3. DATES COVERED</b> 30 Sep 2014 – 29 Sep 2017	
<b>4. TITLE AND SUBTITLE</b> Understanding and Targeting Tumor Microenvironment in Prostate  Cancer to Inhibit Tumor Progression and Castration Resistance				<b>5a. CONTRACT NUMBER</b>	
				<b>5b. GRANT NUMBER</b> W81XWH-14-1-0576	
				<b>5c. PROGRAM ELEMENT NUMBER</b>	
<b>6. AUTHOR(S)</b>  Yaoqi Alan Wang  E-Mail: <a href="mailto:xlu3@mdanderson.org">xlu3@mdanderson.org</a> ; <a href="mailto:xlu@nd.edu">xlu@nd.edu</a>				<b>5d. PROJECT NUMBER</b>	
				<b>5e. TASK NUMBER</b>	
				<b>5f. WORK UNIT NUMBER</b>	
<b>7. PERFORMING ORGANIZATION NAME(S) AND ADDRESS(ES)</b>  MD Anderson Cancer Center 3SCR5.4410, 1881 East Road Houston, TX, 7054				<b>8. PERFORMING ORGANIZATION REPORT NUMBER</b>	
<b>9. SPONSORING / MONITORING AGENCY NAME(S) AND ADDRESS(ES)</b> U.S. Army Medical Research and Materiel Command Fort Detrick, Maryland 21702n 5012				<b>10. SPONSOR/MONITOR'S ACRONYM(S)</b>	
				<b>11. SPONSOR/MONITOR'S REPORT NUMBER(S)</b>	
<b>12. DISTRIBUTION / AVAILABILITY STATEMENT</b>  Approved for Public Release; Distribution Unlimited					
<b>13. SUPPLEMENTARY NOTES</b>					
<b>14. ABSTRACT</b> A significant fraction of advanced prostate cancer (PCa) patients treated with androgen deprivation therapy (ADT) experience relapse with relentless progression to lethal metastatic castration-resistant prostate cancer (mCRPC). Immune checkpoint blockade (ICB) using antibodies against CTLA4 or PD1/PD-L1 generates durable therapeutic responses in a significant subset of patients across a variety of cancer types. However, mCRPC showed overwhelming de novo resistance to ICB, motivating a search for targeted therapies that overcome this resistance. Myeloid-derived suppressor cells (MDSCs) are known to play important roles in tumor immune evasion. Circulating MDSC abundance correlates with PSA levels and metastasis in PCa patients. Mouse models of PCa show that MDSCs (CD11b+ Gr1+) promote tumor initiation and progression. These observations prompted us to hypothesize that robust immunotherapy responses in mCRPC may be elicited by the combined actions of ICB agents together with targeted agents that neutralize MDSCs yet preserve T cell function. Here I developed a novel chimeric mouse model of mCRPC to efficiently test combination therapies in an autochthonous setting. Combination of anti-CTLA4 and anti-PD1 engendered only modest efficacy. Targeted therapy against mCRPC-infiltrating MDSCs, using multikinase inhibitors such as cabozantinib and dactolisib, also showed minimal anti-tumor activities. Strikingly, primary and metastatic CRPC showed robust synergistic responses when ICB was combined with MDSC-targeted therapy. Mechanistically, combination therapy efficacy stemmed from the upregulation of IL-1ra and suppression of MDSC-promoting cytokines secreted by PCa cells. These observations illuminate a clinical path hypothesis for combining ICB with MDSC-targeted therapies in the treatment of mCRPC.					
<b>15. SUBJECT TERMS</b> Prostate cancer, metastatic castration-resistant prostate cancer (mCRPC), androgen deprivation therapy (ADT), immune checkpoint blockade (ICB), myeloid-derived suppressor cell (MDSC), Pten, Smad4, p53, YAP, CXCR2, CTLA4, PD1, cabozantinib, BEZ235, chimeric mouse modeling, combination therapy					
<b>16. SECURITY CLASSIFICATION OF:</b>			<b>17. LIMITATION OF ABSTRACT</b>  Unclassified	<b>18. NUMBER OF PAGES</b>  28	<b>19a. NAME OF RESPONSIBLE PERSON</b> USAMRMC
<b>a. REPORT</b>  Unclassified	<b>b. ABSTRACT</b>  Unclassified	<b>c. THIS PAGE</b>  Unclassified			<b>19b. TELEPHONE NUMBER (include area code)</b>

## Table of Contents

	<u>Page</u>
<b>1. Introduction.....</b>	<b>4</b>
<b>2. Keywords.....</b>	<b>4</b>
<b>3. Accomplishments.....</b>	<b>4</b>
<b>4. Impact.....</b>	<b>8</b>
<b>5. Changes/Problems.....</b>	<b>N/A</b>
<b>6. Products.....</b>	<b>9</b>
<b>7. Participants &amp; Other Collaborating Organizations.....</b>	<b>9</b>
<b>8. Special Reporting Requirements.....</b>	<b>10</b>
<b>9. Appendices.....</b>	<b>10</b>

## 1. INTRODUCTION

Through the 3 years of funding, I have focused on identifying the pro-tumor function and mechanism of myeloid derived suppressor cells (MDSCs) in transgenic mouse models of prostate tumor and determining that combination of MDSC-targeting reagents with immune checkpoint blockade (ICB) induces synergistic efficacy in treating aggressive PCa. A significant fraction of advanced PCa patients treated with androgen deprivation therapy (ADT) experience relapse with relentless progression to lethal metastatic castration-resistant prostate cancer (mCRPC)<sup>1</sup>. ICB using antibodies against cytotoxic-T-lymphocyte-associated protein 4 (CTLA4) or programmed cell death 1/ programmed cell death 1 ligand 1 (PD1/PD-L1) generates durable therapeutic responses in a significant subset of patients across a variety of cancer types<sup>2</sup>. However, mCRPC showed overwhelming *de novo* resistance to ICB<sup>3-5</sup>, motivating a search for targeted therapies that overcome this resistance. MDSCs are known to play important roles in tumor immune evasion<sup>6</sup>. Circulating MDSC abundance correlates with PSA levels and metastasis in PCa patients<sup>7-9</sup>. Mouse models of PCa show that MDSCs (CD11b<sup>+</sup> Gr1<sup>+</sup>) promote tumor initiation<sup>10</sup> and progression<sup>11</sup>. These observations prompted me to hypothesize that robust immunotherapy responses in mCRPC may be elicited by the combined actions of ICB agents together with targeted agents that neutralize MDSCs yet preserve T cell function.

## 2. KEYWORDS

Prostate cancer, metastatic castration-resistant prostate cancer, immune checkpoint blockade, myeloid-derived suppressor cell, cabozantinib, BEZ235, chimeric mouse modeling

## 3. ACCOMPLISHMENTS

### ○ What were the major goals of the project?

Goal 1: Identify the function and molecular mechanism of MDSCs in PCa progression

Goal 2: Develop combination immunotherapy strategy based on co-targeting MDSCs and immune checkpoints

### ○ What was accomplished under these goals?

Through Year 1 and Year 2, I accomplished the majority of the experiments proposed in the three Aims in the original Narrative and SOW. In Year 3, I accomplished the aims and experiments outlined in the revised SOW. Importantly, under the support from this grant, I published two high-impact papers (Cancer Discover, 2016; Nature, 2017)<sup>11,12</sup>. Both publications were well received by the prostate cancer research community, demonstrated by the invitation to present journal club webinars for both papers at Prostate Cancer Foundation (PCF). The Nature publication was also highlighted by CDMRP at its website [http://cdmrp.army.mil/pcrp/research\\_highlights/17xin\\_lu\\_highlight](http://cdmrp.army.mil/pcrp/research_highlights/17xin_lu_highlight). Below I will describe my accomplishments in Year 3 with figures and tables referenced to my Nature paper published in 2017 (attached as Appendix in this report).

Mouse models of PCa engineered with signature mutations of human PCa exhibit autochthonous tumor evolution in an intact immune system<sup>13-15</sup>. However, traditional germline genetic modeling has limited capacity to generate the cohort sizes needed to conduct multi-arm drug testing. This issue is particularly pressing for PCa models based on *PB-Cre*<sup>13</sup> with optimal intercrosses producing 12.5% PCa-prone males (**Extended Data Fig. 1a**). Here, we employed a novel non-germline mCRPC model in a C57BL/6 background through first establishing JH61 and JH58 mouse embryonic stem cell (mESC) clones (**Extended Data Fig. 1b-d**) derived from the following genotypes: *PB-Cre*<sup>+</sup> *Pten*<sup>L/L</sup> *p53*<sup>L/L</sup> *Smad4*<sup>L/L</sup> *mTmG*<sup>L/+</sup> *LSL-LUC*<sup>L/+</sup> (CPPSML) which exhibited age-dependent GFP<sup>+</sup>LUC<sup>+</sup> PCa development (**Fig. 1a**). In high percentage chimeras derived from JH61 or JH58 mESCs (**Extended Data Table 1a**), 50% of mice (4/8 necropsied) developed GFP<sup>+</sup> cancer cells at 3 months of age and showed dissemination of cancer cells to draining lymph nodes (LN) and lung (**Extended Data Fig. 1e-1f**). In prostate, GFP<sup>+</sup> areas corresponded to CK8<sup>+</sup>/CK5<sup>+</sup> adenocarcinoma (**Extended Data Fig. 1g-h**). Importantly, we observed a 4-fold increase in the rate by which PCa-bearing mice can be generated using chimeric modeling (**Extended Data Fig. 1a**). To study combination therapy targeting mCRPC, we first employed the *PB-Cre*<sup>+</sup> *Pten*<sup>L/L</sup> *p53*<sup>L/L</sup> *Smad4*<sup>L/L</sup> germline model and demonstrated that an ADT protocol

(castration followed by enzalutamide-admixed diet) generated a significant, albeit transient, survival benefit (**Extended Data Fig. 2a**). Next, CPPSML chimeras were subjected to the same ADT to induce CRPC. To ensure consistency, MRI was used to enroll chimeras with prostate tumor volumes over 150mm<sup>3</sup> before 18 weeks of age – 86/107 (80.4%) chimeras met this criterion (**Fig. 1b, Extended Data Fig. 2b**). We validated emergence of CRPC in CPPSML chimeras by comparing the response of size-matched primary prostate tumors to ADT in three cohorts: the chimeras, CPPSML mice through breeding, and castration-sensitive *PB-Cre<sup>+</sup>Pten<sup>L/L</sup>* mice (**Fig. 1c**). All treated chimeras succumbed to primary CRPC, with metastases in LN and micrometastases in lungs (**Extended Data Fig. 2c**). Thus, the CPPSML chimera models provide a speedy platform to test multiple therapies on mCRPC.

Next, mCRPC-bearing chimera mice were enlisted into therapeutic trials. The targeted agents were selected on the basis of (i) strong activity in preclinical PCa models, (ii) initial activity and safety in early phase trials but failure to improve overall survival in Phase III trials of mCRPC, and/or (iii) purported immunomodulatory activities and thus the potential to enhance or negate ICB. The agents selected were the tyrosine kinase inhibitors dasatinib (Dasa)<sup>16</sup> and cabozantinib (Cabo)<sup>17</sup>, and the PI3K/mTOR dual inhibitor BEZ235 (BEZ)<sup>18,19</sup>. Of relevance to this study, previous evidence suggests that PI3K pathway activation in both cancer cells and cancer associated myeloid cells can mediate immunosuppression<sup>20-24</sup> and that BEZ exhibits minimal inhibitory activity on mouse T cells<sup>25</sup>. For ICB, we utilized a cocktail of anti-CTLA4 and anti-PD1 antibodies to maximize the blockade of checkpoint pathways, a regimen in line with a clinical treatment protocol currently being tested in a Phase II trial for mCRPC (NCT02601014). CPPSML chimeras (generated from JH61) with induced and MRI-documented mCRPC were randomized to receive single or combination treatments for 4 weeks before endpoint analysis (**Extended Data Fig. 2d**). While all targeted agent monotherapies or dual ICB cocktail had minimal impact on prostate tumor weight, the combination of Cabo + ICB or BEZ + ICB showed potent synergistic efficacy in targeting primary and metastatic PCa growth (**Fig. 1d-f, Extended Data Fig. 2e**). In contrast, ICB alone or Dasa + ICB showed minimal impact on primary or metastatic disease burden, although ICB alone resulted in significant reduction of LN metastasis and lung micrometastasis (**Fig. 1d-f, Extended Data Fig. 2e**). In a corroborating study with chimeras derived from JH58, Cabo + ICB also generated significant efficacy in the mCRPC setting (**Extended Data Fig. 3a-c**). At necropsy, Cabo + ICB and BEZ + ICB treated CRPC mice showed minimal residual tumor cells in the prostate (**Extended Data Fig. 2e**), reduced proliferation and pronounced apoptosis (**Extended Data Fig. 3d-g**).

We catalogued the constellation of intratumoral immunocytes by CyTOF<sup>11</sup> in the various treatment arms as part of end-point analyses. Continued Dasa, but not Cabo or BEZ, treatment was associated with a significant reduction of tumor infiltrating T cells (**Extended Data Fig. 4a**), suggesting that the meager impact of Dasa + ICB may reflect depletion of T cells in the tumor microenvironment (TME). This finding is consistent with reported Dasa inhibition of TCR-mediated signal transduction and proliferation<sup>26</sup>. CPPSML PCa tumors predominantly contain granulocytic MDSCs (Gr-MDSCs, CD11b<sup>+</sup>Gr1<sup>+</sup>Ly6G<sup>+</sup>Ly6C<sup>low</sup>) (**Extended Data Fig. 4b**). Either Cabo or BEZ treatment resulted in a significant reduction of Gr-MDSCs, while ICB alone had no impact (**Fig. 2a**). However, ICB significantly increased CD8<sup>+</sup>/T<sub>reg</sub> ratio (**Fig. 2b**), a defining feature for ICB-based therapies. Cabo + ICB and BEZ + ICB further elevated CD8<sup>+</sup>/T<sub>reg</sub> ratios (**Fig. 2b**). MDSC depletion with anti-Gr1 neutralizing antibody<sup>11</sup> sensitized CRPC in CPPSML to ICB (**Extended Data Fig. 4c**), arguing that MDSCs mediate *de novo* resistance to ICB and suggesting that Cabo or BEZ enhances ICB through diminishing MDSCs.

To explore the impact of these agents on cells in the TME, *in vitro* viability assays were performed to audit Cabo, BEZ and Dasa activity on MDSCs, CD8<sup>+</sup> T cells, and GFP<sup>+</sup> PCa cells harvested from CRPC in CPPSML. Relative to CD8<sup>+</sup> T cells and GFP<sup>+</sup> PCa cells, MDSCs displayed a significantly higher sensitivity to Cabo and BEZ, but not to Dasa (**Fig. 2c-d, Extended Data Fig. 5a**). Similar IC<sub>50</sub> results were obtained when MDSCs were assayed in medium supplemented with 10ng/ml GM-CSF (**Extended Data Fig. 5b**) or in medium supplemented with GM-CSF and also pre-conditioned for 12 hours by PCa cell lines established from the CPPSML model (**Extended Data Fig. 5c**). Moreover, Cabo or BEZ treatment alleviated the suppressive activity of intratumoral MDSCs on CD4<sup>+</sup> and CD8<sup>+</sup> T cell proliferation (**Fig. 2e, Extended Data Fig. 5d**). On the other hand, CD8<sup>+</sup> and CD4<sup>+</sup> T cell *in vitro* proliferation was only moderately suppressed by Cabo or BEZ, yet completely blocked by Dasa (**Fig. 2f-g, Extended Data Fig. 5e**). Equivalent drug effects on IFN- $\gamma$  and IL-2

production by T cells were observed (**Fig. 2h-i**). In summary, Cabo and BEZ elicited pronounced effect on the infiltration and activity of MDSCs.

Next, phospho-receptor tyrosine kinase (RTK) antibody arrays were used to assess the effect of Cabo and BEZ on the RTK signaling in treated CPPSML tumors (**Extended Data Fig. 6a**), revealing Cabo-induced downregulation of pEGFR, pErbB2, pErbB3, pAxl, and pPDGFR $\alpha$ , and partial downregulation of pEGFR, pErbB3, and pAxl through indirect effect by BEZ (**Fig. 3a**). We further observed that Cabo or BEZ also reduced pMET and pVEGFR2 levels, and significantly suppressed PI3K-Akt-mTOR signaling in CPPSML tumors (**Fig. 3b**). Correspondingly, Cabo or BEZ decreased pS6 signaling in intratumoral Gr1<sup>+</sup> MDSCs in the CPPSML TME (**Extended Data Fig. 6b-c**). These findings raised the possibility that Cabo and BEZ compromise MDSCs through inhibition of PI3K signaling. To test this hypothesis, we sought to rescue the viability of Cabo- or BEZ-treated MDSCs with enforced downstream activation of signaling surrogates. Specifically, MDSCs were isolated from the induced CRPC in CPPSML and co-transfected with recombinant active ERK2 and p70S6K proteins (**Fig. 3c**). Transfected MDSCs showed improved survival under Cabo or BEZ treatment (**Fig. 3d-e**). Similar results were obtained when the assay was performed in enhanced medium (**Extended Data Fig. 6d-e**). These results reinforce the view that Cabo and BEZ exert an impact on the PCa TME in part via selective depletion of MDSCs.

As cytokine signaling plays a pivotal role in the recruitment and activation of MDSCs<sup>6</sup>, we further explored the impact of combination treatment on cytokine production in primary CRPC. Cytokine arrays revealed that several key cytokines involved in regulating recruitment and activity of immunosuppressive myeloid cells, including CCL5, CCL12, CD40 and HGF, were reduced by Cabo + ICB or BEZ + ICB treatment. These treatments were also associated with increased IL-1ra, CD142, and VEGF (**Fig. 3f, Extended Data Fig. 7a**). IL-1ra may contribute to reduced MDSC infiltration<sup>27</sup>. We confirmed that recombinant IL-1ra inhibited IL-1 induced chemoattraction of MDSCs, and this effect was blocked by IL-1ra neutralizing antibody (**Fig. 3g**). Notably, the cytokine changes were significantly less pronounced in Dasa + ICB treatment (**Extended Data Fig. 7b**). Noting that cytokine production by cancer cells may influence the functional status of myeloid cells, we cultured MDSCs isolated from CRPC with conditioned medium from the CPPSML PCa cell lines (**Extended Data Fig. 7c**) and showed upregulated expression of genes responsible for MDSC-induced immune suppression, including *Arg1*, *Cybb*, *Ncf1*, and *Ncf4*<sup>6,11</sup> (**Fig. 3h**). Critically, the expression induction was largely abolished if the PCa cells were pre-treated with Cabo or BEZ before conditioned medium was collected (**Fig. 3i**), whereas direct treatment of MDSCs with Cabo or BEZ caused insignificant expression changes (data not shown), suggesting that certain cytokines in the conditioned medium may drive the gene upregulation. Through cytokine array (**Extended Data Fig. 7d**), we identified 10 cytokines significantly downregulated in the conditioned medium of PCa cells pre-treated with Cabo or BEZ (**Fig. 3j**), among which CCL5 was also identified as a downregulated cytokine in Cabo + ICB and BEZ + ICB treated CRPC (**Fig. 3f**). When MDSCs isolated from CRPC tumors were treated with each of the 10 cytokines in the presence of Cabo or BEZ, significant upregulation of *Arg1*, *Cybb*, *Ncf1* and *Ncf4* was observed with most of the cytokines tested (**Extended Data Fig. 7e**). Therefore, PCa cells are capable of driving immunosuppression-related gene expression in MDSCs through secretion of multiple cytokines, and this paracrine signaling is impaired by Cabo or BEZ treatment.

BEZ targets multiple p110 isoforms. To test if isoform-specific PI3K inhibitors would generate a comparable level of synergistic advantage when combined with ICB, we tested PI-3065 (p110 $\delta$ -selective inhibitor<sup>28</sup>) and GSK2636771 (p110 $\beta$ -selective inhibitor<sup>29</sup>). Moreover, given the critical role of Cxcr2 in MDSC recruitment<sup>10,11</sup> and the downregulation of Cxcr2 ligands Cxcl1 and Cxcl2 in the conditioned medium of PCa cells treated with Cabo and BEZ (**Fig. 3j**), we also tested a novel clinical-stage Cxcr1/2 inhibitor SX-682 (**Extended Data Fig. 7f-g**) as monotherapy or in combination with ICB in the CPPSML model. Meager to moderate effects of PI-3065, GSK2636771 or SX-682 as single agents on CRPC progression was observed, yet combination with ICB produced strong efficacy (**Fig. 4a-b**). To further credential our model and assess the pattern of MDSCs in human PCa, a 32-antibody CyTOF panel was developed (**Extended Data Table 1b**) and used to analyze 12 fresh fine needle biopsy samples from 10 treatment-naïve PCa tumors (**Extended Data Table 1c**). SPADE analysis displayed the heterogeneous immune cell populations (**Extended Data Fig. 8**). Results showed the prominence of Gr-MDSCs relative to Mo-MDSCs, with the latter occupying no nodes in the

SPADE tree (**Fig. 4c**). Total T cell load across the samples varied considerably (**Fig. 4d**), yet the frequency of CD8<sup>+</sup> T cells correlated inversely with the frequency of Gr-MDSCs (**Fig. 4e**), a pattern consistent with the conservation of antagonistic activity of Gr-MDSCs to CD8<sup>+</sup> T cells in human PCa.

Based on my DOD-supported research, I was successful to land an independent assistant professor job at the University of Notre Dame, starting Jan 2017. For my independent research program at University of Notre Dame, I am excited to lead my laboratory to focus on innovative and impactful research projects in the area of tumor immunology and immunotherapy.

## References

- 1 Watson, P. A., Arora, V. K. & Sawyers, C. L. Emerging mechanisms of resistance to androgen receptor inhibitors in prostate cancer. *Nat Rev Cancer* 15, 701-711 (2015).
- 2 Sharma, P. & Allison, J. P. The future of immune checkpoint therapy. *Science* 348, 56-61 (2015).
- 3 Kwon, E. D. *et al.* Ipilimumab versus placebo after radiotherapy in patients with metastatic castration-resistant prostate cancer that had progressed after docetaxel chemotherapy (CA184-043): a multicentre, randomised, double-blind, phase 3 trial. *The Lancet Oncology* 15, 700-712 (2014).
- 4 Beer, T. M. *et al.* Randomized, Double-Blind, Phase III Trial of Ipilimumab Versus Placebo in Asymptomatic or Minimally Symptomatic Patients With Metastatic Chemotherapy-Naive Castration-Resistant Prostate Cancer. *Journal of Clinical Oncology* 35, 40-47 (2017).
- 5 Topalian, S. L. Safety, activity, and immune correlates of anti-PD-1 antibody in cancer. *N. Engl. J. Med.* 366, 2443-2454 (2012).
- 6 Gabrilovich, D. I. & Nagaraj, S. Myeloid-derived suppressor cells as regulators of the immune system. *Nat Rev Immunol* 9, 162-174 (2009).
- 7 Vuk-Pavlović, S. *et al.* Immunosuppressive CD14+HLA-DR<sup>low</sup>/- monocytes in prostate cancer. *Prostate* 70, 443-455 (2010).
- 8 Brusa, D. *et al.* Circulating immunosuppressive cells of prostate cancer patients before and after radical prostatectomy: Profile comparison. *Int J Urol* 2013, 12086 (2013).
- 9 Hossain, D. M. *et al.* TLR9-Targeted STAT3 Silencing Abrogates Immunosuppressive Activity of Myeloid-Derived Suppressor Cells from Prostate Cancer Patients. *Clin Cancer Res* 21, 3771-3782 (2015).
- 10 Di Mitri, D. *et al.* Tumour-infiltrating Gr-1+ myeloid cells antagonize senescence in cancer. *Nature* 515, 134-137 (2014).
- 11 Wang, G. *et al.* Targeting YAP-Dependent MDSC Infiltration Impairs Tumor Progression. *Cancer Discov* 6, 80-95 (2016).
- 12 Lu, X. *et al.* Effective combinatorial immunotherapy for castration-resistant prostate cancer. *Nature* 543, 728-732 (2017).
- 13 Shen, M. M. & Abate-Shen, C. Molecular genetics of prostate cancer: new prospects for old challenges. *Genes & Development* 24, 1967-2000 (2010).
- 14 Ding, Z. *et al.* Telomerase reactivation following telomere dysfunction yields murine prostate tumors with bone metastases. *Cell* 148, 896-907 (2012).
- 15 Ding, Z. *et al.* SMAD4-dependent barrier constrains prostate cancer growth and metastatic progression. *Nature* 470, 269-273 (2011).
- 16 Araujo, J. C. *et al.* Docetaxel and dasatinib or placebo in men with metastatic castration-resistant prostate cancer (READY): a randomised, double-blind phase 3 trial. *The Lancet Oncology* 14, 1307-1316 (2013).
- 17 Smith, M. *et al.* Phase III Study of Cabozantinib in Previously Treated Metastatic Castration-Resistant Prostate Cancer: COMET-1. *Journal of Clinical Oncology* (2016).
- 18 Carver, Brett S. *et al.* Reciprocal Feedback Regulation of PI3K and Androgen Receptor Signaling in PTEN-Deficient Prostate Cancer. *Cancer Cell* 19, 575-586 (2011).
- 19 Jia, S. *et al.* Opposing effects of androgen deprivation and targeted therapy on prostate cancer prevention. *Cancer Discov* 3, 44-51 (2013).

- 20 Peng, W. *et al.* Loss of PTEN Promotes Resistance to T Cell-Mediated Immunotherapy. *Cancer Discov* 6, 202-216 (2016).
- 21 Kim, K. *et al.* Eradication of metastatic mouse cancers resistant to immune checkpoint blockade by suppression of myeloid-derived cells. *Proceedings of the National Academy of Sciences* 111, 11774-11779 (2014).
- 22 Rivera, Lee B. *et al.* Intratumoral Myeloid Cells Regulate Responsiveness and Resistance to Antiangiogenic Therapy. *Cell Reports* 11, 577-591 (2015).
- 23 De Henau, O. *et al.* Overcoming resistance to checkpoint blockade therapy by targeting PI3K $\gamma$  in myeloid cells. *Nature* 539, 443-447 (2016).
- 24 Kaneda, M. M. *et al.* PI3K $\gamma$  is a molecular switch that controls immune suppression. *Nature* 539, 437-442 (2016).
- 25 Frick, A. *et al.* Immune cell-based screening assay for response to anticancer agents: applications in pharmacogenomics. *Pharmacogenomics and personalized medicine* 8, 81-98 (2015).
- 26 Schade, A. E. *et al.* Dasatinib, a small-molecule protein tyrosine kinase inhibitor, inhibits T-cell activation and proliferation. *Blood* 111, 1366-1377 (2008).
- 27 Tu, S. *et al.* Overexpression of Interleukin-1 $\beta$  Induces Gastric Inflammation and Cancer and Mobilizes Myeloid-Derived Suppressor Cells in Mice. *Cancer Cell* 14, 408-419 (2008).
- 28 Ali, K. *et al.* Inactivation of PI(3)K p110[dgr] breaks regulatory T-cell-mediated immune tolerance to cancer. *Nature* 510, 407-411 (2014).
- 29 Costa, C. *et al.* Measurement of PIP3 Levels Reveals an Unexpected Role for p110 $\beta$  in Early Adaptive Responses to p110 $\alpha$ -Specific Inhibitors in Luminal Breast Cancer. *Cancer Cell* 27, 97-108 (2015).

○ **What opportunities for training and professional development has the project provided?**

**Professional development:** With the conducted research supported by the grant, the PI Xin Lu had the opportunity for the following conferences and workshops:

- 1) BD Biosciences course “Multicolor Flow Cytometry - Beyond the Basics”. **Certificate awarded.** Sep 16-18, 2014. San Jose, CA
- 2) Society For Immunotherapy of Cancer (SITC) Annual Meeting. Nov 6-9, 2014, National Harbor, MD
- 3) 22nd Annual Prostate Cancer Foundation (PCF) Scientific Retreat. **Poster presentation.** Oct 8-10, 2015. Washington, DC
- 4) American Physical Society March Meeting, **Invited speaker.** Mar 18, 2016. Baltimore, MD
- 5) DoD Prostate Cancer Research Program (PCRP) IMPaCT 2016 conference, **Oral presentation.** Aug 4-5, 2016. Towson, MD
- 6) Symposia on Cancer Research, MD Anderson Cancer Center, Houston, TX, **Oral presentation,** 2016
- 7) Prostate Cancer Foundation (webinar), **Oral presentation,** 2017

○ **How were the results disseminated to communities of interest?**

Under the support from this grant, I published two high-impact papers (Cancer Discover, 2016; Nature, 2017). Both publications were well received by the prostate cancer research community, demonstrated by the invitation to present journal club webinars for both papers at Prostate Cancer Foundation (PCF). The Nature publication was also highlighted by CDMRP at its website [http://cdmrp.army.mil/pcrp/research\\_highlights/17xin\\_lu\\_highlight](http://cdmrp.army.mil/pcrp/research_highlights/17xin_lu_highlight)

#### 4. IMPACT

○ **What was the impact on the development of the principal discipline(s) of the project?**

My results, published in *Cancer Discovery* and *Nature*, have made important contribution to the fields of prostate cancer and tumor microenvironment. The results show that prostate cancer progression is significantly regulated by MDSCs, and targeting MDSCs emerges as an effective method to inhibit aggressive prostate cancer.

- **What was the impact on other disciplines?**

My publications illuminate a clinical path hypothesis for combining immune checkpoint blocking antibodies with MDSC-targeted therapies in the treatment of metastatic CRPC.

- **What was the impact on technology transfer?**

Nothing to Report

- **What was the impact on society beyond science and technology?**

Contribution to and positive impact on the mission of CDMRP PCRCP to end morbidity and mortality caused by aggressive prostate cancer.

## 5. PRODUCTS

### Publications

Wang, G\*, Lu, X\*., Dey, P., Deng, P., Wu, C. C., Jiang, S., Fang, Z., Zhao, K., Konaparthi, R., Hua, S., *et al.* (2016). Targeting YAP-Dependent MDSC Infiltration Impairs Tumor Progression. *Cancer Discov* 6, 80-95. (\*Equal contribution)

Lu X, Horner JW, Paul E, Shang X, Troncoso P, Deng P, Jiang S, Chang Q, Varma A, Han JW, Spring DJ, Sharma P, Zebala JA, Maeda DY, Wang YA, and DePinho RA. Effective Combinatorial Immunotherapy for Metastatic Castration-Resistant Prostate Cancer. *Nature*. 2017; 543:728-732.

## 6. PARTICIPANTS & OTHER COLLABORATING ORGANIZATIONS

- **What individuals have worked on the project?**

Name:	<i>Xin Lu</i>
Project Role:	<i>Instructor</i>
Researcher Identifier (e.g. ORCID ID):	<i>189447 (MD Anderson Cancer Center Employee ID)</i>
Nearest person month worked:	<i>12</i>
Contribution to Project:	<i>No change</i>
Funding Support:	<i>No change</i>
Name:	<i>Guocan Wang</i>
Project Role:	<i>Postdoc Fellow</i>
Researcher Identifier (e.g. ORCID ID):	<i>Not applicable</i>
Nearest person month worked:	<i>6</i>
Contribution to Project:	<i>Dr. Wang has co-performed the works on identification and validation of YAP signaling, as well as part of the clinical validation studies. Dr. Wang also contributed equally to the writing and revision of the manuscript in Cancer Discovery.</i>
Funding Support:	<i>Prostate Cancer Research Program (PCRCP) W81XWH-13-1-0202</i>

- **Has there been a change in the active other support of the PD/PI(s) or senior/key personnel since the last reporting period?**

Nothing to report.

- **What other organizations were involved as partners?**

Nothing to report.

## **7. SPECIAL REPORTING REQUIREMENTS**

Nothing to report.

## **8. APPENDICES:**

Lu X, Horner JW, Paul E, Shang X, Troncoso P, Deng P, Jiang S, Chang Q, Varma A, Han JW, Spring DJ, Sharma P, Zebala JA, Maeda DY, Wang YA, and DePinho RA. Effective Combinatorial Immunotherapy for Metastatic Castration-Resistant Prostate Cancer. *Nature*. 2017; 543:728-732.

## Effective combinatorial immunotherapy for castration-resistant prostate cancer

Xin Lu<sup>1</sup>†, James W. Horner<sup>2</sup>, Erin Paul<sup>2</sup>, Xiaoying Shang<sup>1</sup>, Patricia Troncoso<sup>3</sup>, Pingna Deng<sup>1</sup>, Shan Jiang<sup>2</sup>, Qing Chang<sup>2</sup>, Denise J. Spring<sup>1</sup>, Padmanee Sharma<sup>4</sup>, John A. Zebala<sup>5</sup>, Dean Y. Maeda<sup>5</sup>, Y. Alan Wang<sup>1</sup> & Ronald A. DePinho<sup>1</sup>

A significant fraction of patients with advanced prostate cancer treated with androgen deprivation therapy experience relapse with relentless progression to lethal metastatic castration-resistant prostate cancer (mCRPC)<sup>1</sup>. Immune checkpoint blockade using antibodies against cytotoxic-T-lymphocyte-associated protein 4 (CTLA4) or programmed cell death 1/programmed cell death 1 ligand 1 (PD1/PD-L1) generates durable therapeutic responses in a significant subset of patients across a variety of cancer types<sup>2</sup>. However, mCRPC showed overwhelming *de novo* resistance to immune checkpoint blockade<sup>3–5</sup>, motivating a search for targeted therapies that overcome this resistance. Myeloid-derived suppressor cells (MDSCs) are known to play important roles in tumour immune evasion<sup>6</sup>. The abundance of circulating MDSCs correlates with prostate-specific antigen levels and metastasis in patients with prostate cancer<sup>7–9</sup>. Mouse models of prostate cancer show that MDSCs (CD11b<sup>+</sup>Gr1<sup>+</sup>) promote tumour initiation<sup>10</sup> and progression<sup>11</sup>. These observations prompted us to hypothesize that robust immunotherapy responses in mCRPC may be elicited by the combined actions of immune checkpoint blockade agents together with targeted agents that neutralize MDSCs yet preserve T-cell function. Here we develop a novel chimaeric mouse

model of mCRPC to efficiently test combination therapies in an autochthonous setting. Combination of anti-CTLA4 and anti-PD1 engendered only modest efficacy. Targeted therapy against mCRPC-infiltrating MDSCs, using multikinase inhibitors such as cabozantinib and BEZ235, also showed minimal anti-tumour activities. Strikingly, primary and metastatic CRPC showed robust synergistic responses when immune checkpoint blockade was combined with MDSC-targeted therapy. Mechanistically, combination therapy efficacy stemmed from the upregulation of interleukin-1 receptor antagonist and suppression of MDSC-promoting cytokines secreted by prostate cancer cells. These observations illuminate a clinical path hypothesis for combining immune checkpoint blockade with MDSC-targeted therapies in the treatment of mCRPC.

Mouse models of prostate cancer (PCa) engineered with signature mutations of human PCa exhibit autochthonous tumour evolution in an intact immune system<sup>12–14</sup>. However, traditional germline genetic modelling has limited capacity in generating the cohort sizes needed to conduct multi-arm drug testing. This issue is particularly pressing for PCa models based on *PB-Cre*<sup>12</sup>, with optimal intercrosses producing 12.5% PCa-prone males (Extended Data Fig. 1a). Here, we employed a

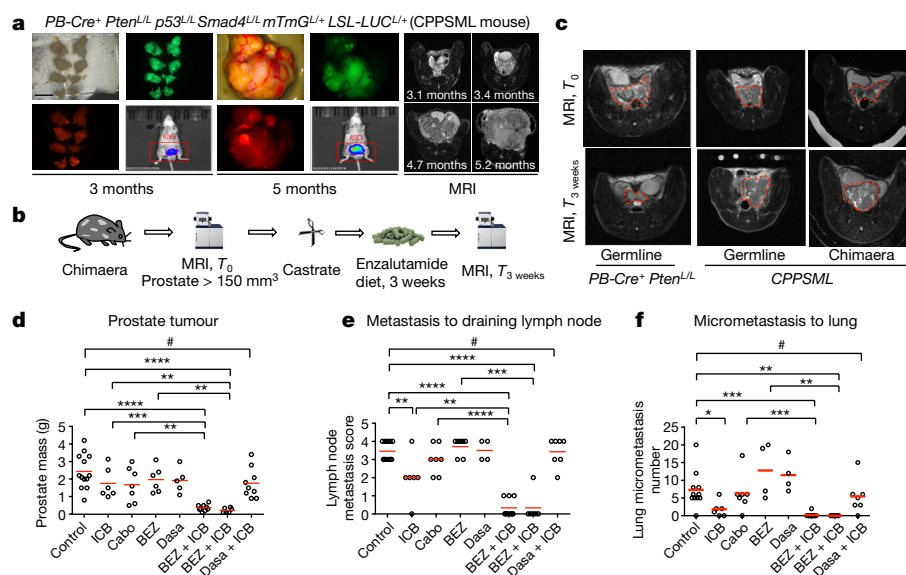


**Figure 1 | Strong combination synergy by ICB with cabozantinib or BEZ235 in mCRPC.** **a**, Spontaneous prostate tumour development in the CPPSML model with tumours detected by fluorescence, bioluminescence, and MRI. Scale bar, 5 mm. **b**, **c**, Procedures and representative MRI images for testing prostate tumour response to castration and enzalutamide diet in

*PB-Cre<sup>+</sup> Pten<sup>L/L</sup>* mice and CPPSML mice ( $n = 5$ , biological replicates). **d–f**, Preclinical trial results of prostate tumour mass, lymph node metastasis score, and lung micrometastasis number ( $n = 11, 6, 7, 4, 4, 9, 6$ , and  $7$ , respectively, biological replicates). Red bar, mean. \* $P < 0.05$ , \*\* $P < 0.01$ , \*\*\* $P < 0.001$ , \*\*\*\* $P < 0.0001$ , # $P > 0.05$ , Mann–Whitney *U*-test.

<sup>1</sup>Department of Cancer Biology, The University of Texas MD Anderson Cancer Center, Houston, Texas 77030, USA. <sup>2</sup>Institute for Applied Cancer Science, The University of Texas MD Anderson Cancer Center, Houston, Texas 77030, USA. <sup>3</sup>Department of Pathology, The University of Texas MD Anderson Cancer Center, Houston, Texas 77030, USA. <sup>4</sup>Department of Genitourinary Medical Oncology, The University of Texas MD Anderson Cancer Center, Houston, Texas 77030, USA. <sup>5</sup>Syntrex Biosystems, Inc., Auburn, Washington 98001, USA. †Present address: Department of Biological Sciences, University of Notre Dame, Notre Dame, Indiana 46556, USA.

novel non-germline mCRPC model in a C57BL/6 background through first establishing JH61 and JH58 mouse embryonic stem cell (mES cell) clones (Extended Data Fig. 1b–d) derived from the following genotypes: *PB-Cre<sup>+</sup> Pten<sup>L/L</sup> p53<sup>L/L</sup> Smad4<sup>L/L</sup> mTmG<sup>L/+</sup> LSL-LUC<sup>L/+</sup>* (CPPSML), which exhibited age-dependent green fluorescent protein (GFP<sup>+</sup>)LUC<sup>+</sup> PCa development (Fig. 1a). In high-percentage chimaeras derived from JH61 or JH58 mES cells (Extended Data Table 1a), 50% of mice (4 out of 8 necropsied) developed GFP<sup>+</sup> cancer cells at 3 months of age and showed dissemination of cancer cells to draining lymph nodes and lung (Extended Data Fig. 1e, f). In prostate, GFP<sup>+</sup> areas corresponded to CK8<sup>+</sup>/CK5<sup>+</sup> adenocarcinoma (Extended Data Fig. 1g, h). Importantly, we observed a fourfold increase in the rate by which PCa-bearing mice can be generated using chimaeric modelling (Extended Data Fig. 1a). To study combination therapy targeting mCRPC, we first employed the *PB-Cre<sup>+</sup> Pten<sup>L/L</sup> p53<sup>L/L</sup> Smad4<sup>L/L</sup>* germline model and demonstrated that an androgen deprivation therapy protocol (castration followed by enzalutamide-admixed diet) generated a significant, albeit transient, survival benefit (Extended Data Fig. 2a). Next, CPPSML chimaeras were subjected to the same androgen deprivation therapy to induce CRPC. To ensure consistency, MRI was used to assign chimaeras with prostate tumour volumes over 150 mm<sup>3</sup> before 18 weeks of age: 86 out of 107 (80.4%) chimaeras met this criterion (Fig. 1b and Extended Data Fig. 2b). We validated emergence of CRPC in CPPSML chimaeras by comparing the response of size-matched primary prostate tumours with androgen deprivation therapy in three cohorts: the chimaeras, CPPSML mice through breeding, and castration-sensitive *PB-Cre<sup>+</sup> Pten<sup>L/L</sup>* mice (Fig. 1c). All treated chimaeras succumbed to primary CRPC, with metastases in lymph nodes and micrometastases in lungs (Extended Data Fig. 2c). Thus, the CPPSML chimaera models provide a speedy platform to test multiple therapies on mCRPC.

Next, mCRPC-bearing chimaera mice were assigned to therapeutic trials. The targeted agents were selected on the basis of (1) strong activity in preclinical PCa models, (2) initial activity and safety in early

phase trials but failure to improve overall survival in phase III trials of mCRPC, and/or (3) purported immunomodulatory activities and thus the potential to enhance or negate immune checkpoint blockade (ICB). The agents selected were the tyrosine kinase inhibitors dasatinib (Dasa)<sup>15</sup> and cabozantinib (Cabo)<sup>16</sup>, and the phosphoinositide 3-kinase (PI3K)/mTOR dual inhibitor BEZ235 (BEZ)<sup>17,18</sup>. Of relevance to this study, previous evidence suggests that PI3K pathway activation in both cancer cells and cancer-associated myeloid cells can mediate immunosuppression<sup>19–23</sup> and that BEZ exhibits minimal inhibitory activity on mouse T cells<sup>24</sup>. For ICB, we used a cocktail of anti-CTLA4 and anti-PD1 antibodies to maximize the blockade of checkpoint pathways, a regimen in line with a clinical treatment protocol currently being tested in a phase II trial for mCRPC (NCT02601014). CPPSML chimaeras (generated from JH61) with induced and MRI-documented mCRPC were randomized to receive single or combination treatments for 4 weeks before endpoint analysis (Extended Data Fig. 2d). While all targeted agent monotherapies or dual ICB cocktail had minimal impact on prostate tumour mass, the combination of Cabo + ICB or BEZ + ICB showed potent synergistic efficacy in targeting primary and metastatic PCa growth (Fig. 1d–f and Extended Data Fig. 2e). In contrast, ICB alone or Dasa + ICB showed minimal impact on primary or metastatic disease burden, although ICB alone resulted in significant reduction of lymph node metastasis and lung micrometastasis (Fig. 1d–f and Extended Data Fig. 2e). In a corroborating study with chimaeras derived from JH58, Cabo + ICB also generated significant efficacy in the mCRPC setting (Extended Data Fig. 3a–c). At necropsy, Cabo + ICB- and BEZ + ICB-treated CRPC mice showed minimal residual tumour cells in the prostate (Extended Data Fig. 2e), reduced proliferation, and pronounced apoptosis (Extended Data Fig. 3d–g).

We catalogued the constellation of intratumoural immunocytes by time of flight mass cytometry (CyTOF)<sup>11</sup> in the various treatment arms as part of end-point analyses. Continued Dasa, but not Cabo or BEZ, treatment was associated with a significant reduction of

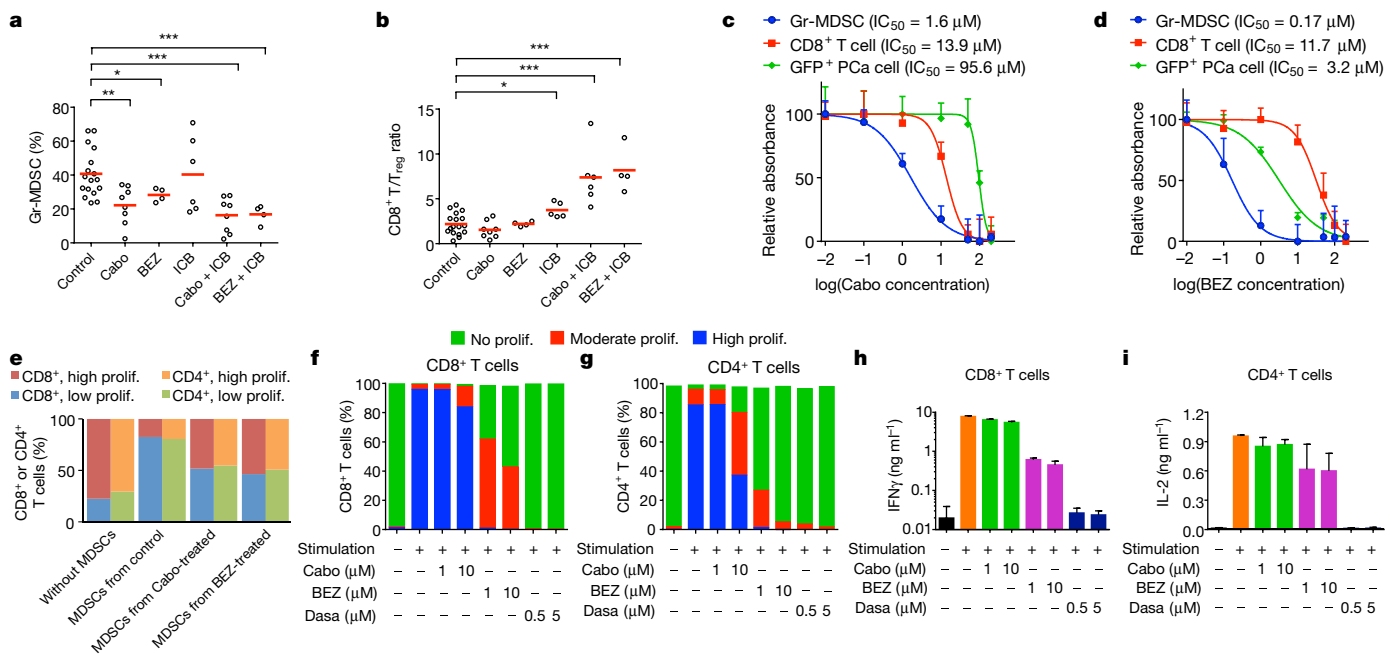


**Figure 2 | Cabozantinib and BEZ235 attenuate MDSC frequency and immunosuppressive activity in the tumour microenvironment.**

**a**, CyTOF quantification of intratumoural Gr-MDSC frequency and CD8<sup>+</sup> T/Reg ratio by indicated treatments ( $n = 17, 8, 4, 6, 8, 8, 4$ , respectively). Red bar, mean. \* $P < 0.05$ , \*\* $P < 0.01$ , \*\*\* $P < 0.001$ , Mann–Whitney  $U$ -test. **c**, **d**, *In vitro* sensitivity to Cabo (**c**) and BEZ (**d**) by MDSCs, CD8<sup>+</sup> T cells, and GFP<sup>+</sup> PCa cells isolated from CRPC in CPPSML mice with IC<sub>50</sub> indicated ( $n = 3$ , biological replicates). **e**, T-cell proliferation (prolif.) assay when co-cultured 1:1 with MDSCs isolated

from control or drug-treated CRPC. High and low proliferation was defined as T-cell division  $\geq 3$  and  $\leq 2$ , respectively ( $n \geq 4$ , biological replicates). **f**, **g**, Drug effect on CD8<sup>+</sup> (**f**) and CD4<sup>+</sup> (**g**) T-cell proliferation assay. High, moderate, and no proliferation was defined as T-cell division  $\geq 3$ ,  $\leq 2$ , and 0, respectively ( $n = 3$ , biological replicates). **h**, **i**, Drug effect on IFN $\gamma$  secretion (by CD8<sup>+</sup> T cells) and IL-2 secretion (by CD4<sup>+</sup> T cells) in the assay in **f** and **g** measured by enzyme-linked immunosorbent assay (ELISA) ( $n = 3$ , biological replicates). In **c**, **d**, **h**, and **i**, data represent mean  $\pm$  s.d.

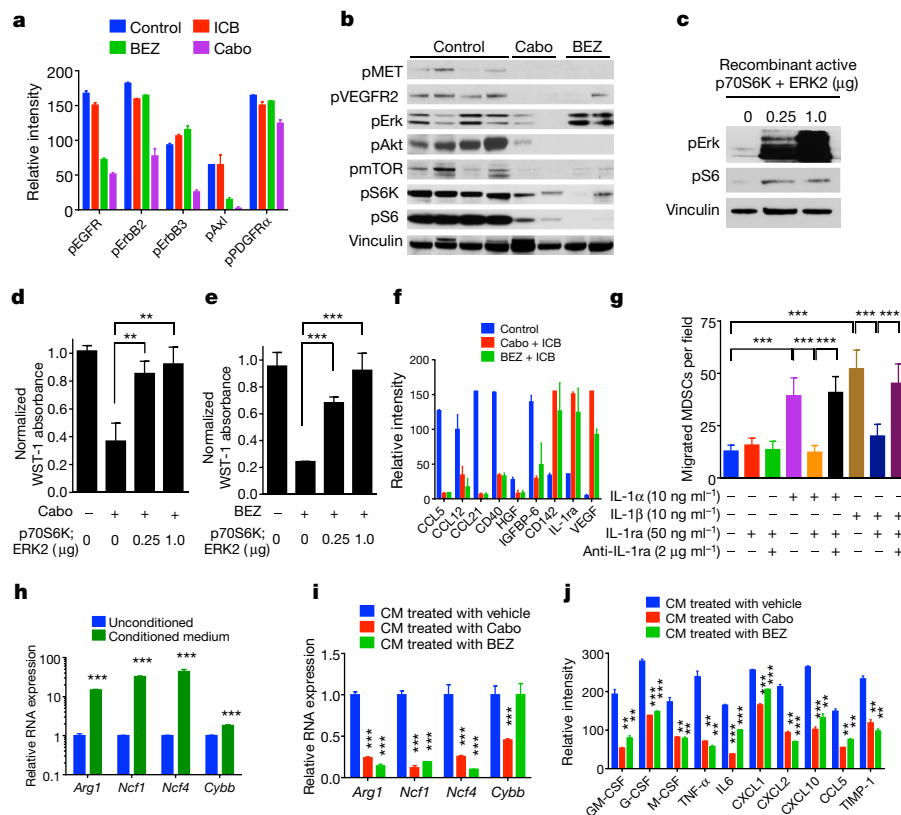


**Figure 3 | Cabozantinib and BEZ235 inhibit PI3K signalling and modulate MDSC-regulating cytokines.** **a**, Relative phospho-RTK intensity measured with phospho-RTK array for treated CRPC ( $n = 2$ , biological replicates). **b**, Level of phospho-proteins in RTK and PI3K–Akt–mTOR pathways in treated tumours, detected with western blot. **c**, p-Erk and p-S6 intensity in MDSCs when co-transfected with ERK2 and p70S6K, detected with western blot. **d**, **e**, Effect of ERK2 and p70S6K on the resistance of MDSCs to Cabo (1.5  $\mu\text{M}$ ) or BEZ (0.15  $\mu\text{M}$ ), measured with WST-1 assay ( $n = 3$ , biological replicates). **f**, Quantification of tumour cytokine levels in treated CRPC using cytokine array ( $n = 2$ , biological replicates). **g**, Trans-well MDSC migration assay ( $n = 3$ , biological replicates). **h**, RNA expression levels of indicated genes by intratumoural MDSCs when cultured in conditioned medium by CPPSML PCa cell lines, measured by quantitative polymerase chain reaction with reverse transcription (qRT–PCR) ( $n = 3$ , biological replicates). **i**, Effect on gene expression by pre-treating CPPSML PCa cells with Cabo and BEZ before conditioned medium was collected to culture MDSCs ( $n = 3$ , biological replicates). **j**, Quantification of cytokine levels in conditioned medium from CPPSML PCa cell lines pre-treated with vehicle, Cabo (1  $\mu\text{M}$ ), or BEZ (1  $\mu\text{M}$ ), measured with cytokine array ( $n = 2$ , biological replicates). In **a** and **d–j**, data represent mean  $\pm$  s.d.  $^{**}P < 0.01$ ,  $^{***}P < 0.001$ , Student's *t*-test. For gel source data, see Supplementary Fig. 1.

replicates). **h**, RNA expression levels of indicated genes by intratumoural MDSCs when cultured in conditioned medium by CPPSML PCa cell lines, measured by quantitative polymerase chain reaction with reverse transcription (qRT–PCR) ( $n = 3$ , biological replicates). **i**, Effect on gene expression by pre-treating CPPSML PCa cells with Cabo and BEZ before conditioned medium was collected to culture MDSCs ( $n = 3$ , biological replicates). **j**, Quantification of cytokine levels in conditioned medium from CPPSML PCa cell lines pre-treated with vehicle, Cabo (1  $\mu\text{M}$ ), or BEZ (1  $\mu\text{M}$ ), measured with cytokine array ( $n = 2$ , biological replicates). In **a** and **d–j**, data represent mean  $\pm$  s.d.  $^{**}P < 0.01$ ,  $^{***}P < 0.001$ , Student's *t*-test. For gel source data, see Supplementary Fig. 1.

tumour-infiltrating T cells (Extended Data Fig. 4a), suggesting that the small impact of Dasa + ICB may reflect depletion of T cells in the tumour microenvironment. This finding is consistent with reported Dasa inhibition of TCR-mediated signal transduction and proliferation<sup>25</sup>. CPPSML PCa tumours predominantly contain granulocytic MDSCs (Gr-MDSCs, CD11b<sup>+</sup>Gr1<sup>+</sup>Ly6G<sup>+</sup>Ly6C<sup>low</sup>) (Extended Data Fig. 4b). Either Cabo or BEZ treatment resulted in a significant reduction of Gr-MDSCs, while ICB alone had no impact (Fig. 2a). However, ICB significantly increased the ratio of CD8<sup>+</sup> to regulatory T cells (T<sub>reg</sub>) (Fig. 2b), a defining feature for ICB-based therapies. Cabo + ICB and BEZ + ICB further elevated CD8<sup>+</sup>/T<sub>reg</sub> ratios (Fig. 2b). MDSC depletion with anti-Gr1 neutralizing antibody<sup>11</sup> sensitized CRPC in CPPSML to ICB (Extended Data Fig. 4c), arguing that MDSCs mediate *de novo* resistance to ICB and suggesting that Cabo or BEZ enhances ICB through diminishing MDSCs.

To explore the impact of these agents on cells in the tumour microenvironment, *in vitro* viability assays were performed to audit Cabo, BEZ, and Dasa activity on MDSCs, CD8<sup>+</sup> T cells, and GFP<sup>+</sup> PCa cells collected from CRPC in CPPSML. Relative to CD8<sup>+</sup> T cells and GFP<sup>+</sup> PCa cells, MDSCs displayed a significantly higher sensitivity to Cabo and BEZ, but not to Dasa (Fig. 2c, d and Extended Data Fig. 5a). Similar half-maximum inhibitory concentration (IC<sub>50</sub>) results were obtained when MDSCs were assayed in medium supplemented with 10 ng ml<sup>-1</sup> granulocyte–macrophage colony-stimulating factor (GM-CSF) (Extended Data Fig. 5b) or in medium supplemented with

GM-CSF and pre-conditioned for 12 h by PCa cell lines established from the CPPSML model (Extended Data Fig. 5c). Moreover, Cabo or BEZ treatment alleviated the suppressive activity of intratumoural MDSCs on CD4<sup>+</sup> and CD8<sup>+</sup> T-cell proliferation (Fig. 2e and Extended Data Fig. 5d). On the other hand, CD8<sup>+</sup> and CD4<sup>+</sup> T-cell *in vitro* proliferation was only moderately suppressed by Cabo or BEZ, yet completely blocked by Dasa (Fig. 2f, g and Extended Data Fig. 5e). Equivalent drug effects on interferon (IFN)- $\gamma$  and interleukin-2 (IL-2) production by T cells were observed (Fig. 2h, i). In summary, Cabo and BEZ elicited a pronounced effect on the infiltration and activity of MDSCs.

Next, phospho-receptor tyrosine kinase (phospho-RTK) antibody arrays were used to assess the effect of Cabo and BEZ on the phospho-RTK signalling in treated CPPSML tumours (Extended Data Fig. 6a), revealing Cabo-induced downregulation of pEGFR, pErbB2, pErbB3, pAkt, and pPDGFR $\alpha$ , and partial downregulation of pEGFR, pErbB3, and pAkt through indirect effect by BEZ (Fig. 3a). We further observed that Cabo or BEZ also reduced phosphorylated MET (pMET) and phosphorylated vascular endothelial growth factor receptor 2 (pVEGFR2) levels, and significantly suppressed PI3K–Akt–mTOR signalling in CPPSML tumours (Fig. 3b). Correspondingly, Cabo or BEZ decreased pS6 signalling in intratumoural Gr1<sup>+</sup> MDSCs in the CPPSML tumour microenvironment (Extended Data Fig. 6b, c). These findings raised the possibility that Cabo and BEZ compromise MDSCs through inhibition of PI3K signalling. To test this hypothesis, we sought to rescue the viability of Cabo- or BEZ-treated MDSCs with

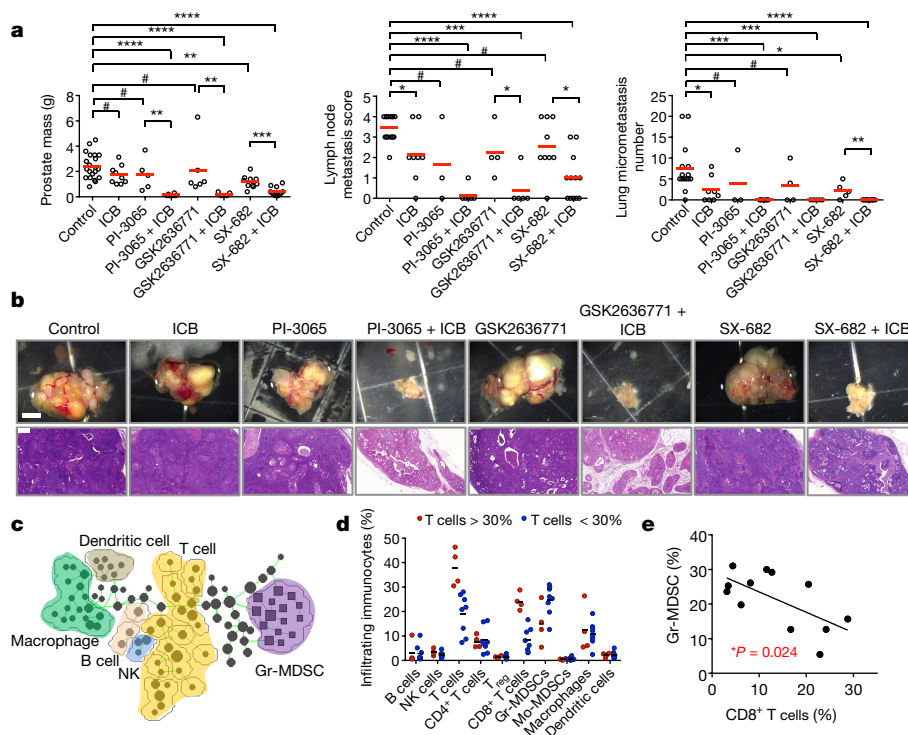


**Figure 4 | Gr-MDSCs inversely correlate with CD8<sup>+</sup> infiltrating T cells in human PCa.** **a, b,** Efficacy of isoform-selective p110 inhibitors or Cxcr1/2 inhibitor as single agents or in combination with ICB to treat mCRPC in CPPSML model ( $n = 15, 8, 3, 6, 4, 5, 5,$  and  $10$  respectively, biological replicates). Red bar, mean. \* $P < 0.05$ , \*\* $P < 0.01$ , \*\*\* $P < 0.001$ , \*\*\*\* $P < 0.0001$ , # $P > 0.05$ , Mann–Whitney  $U$ -test. Scale bars: 3 mm for

organ images, 200  $\mu\text{m}$  for haematoxylin and eosin (H&E) images. **c,** SPADE tree derived from CyTOF analysis of human samples. All live infiltrating immune cells (CD45<sup>+</sup>) were used to construct the tree. NK, natural killer cells. **d,** Frequency of infiltrating immune cell populations from patient samples. **e,** Linear regression analysis of Gr-MDSC frequency with CD8<sup>+</sup> T-cell frequency. In **c–e**,  $n = 12$  (biological replicates).

enforced downstream activation of signalling surrogates. Specifically, MDSCs were isolated from the induced CRPC in CPPSML and co-transfected with recombinant active ERK2 and p70S6K proteins (Fig. 3c). Transfected MDSCs showed improved survival under Cabo or BEZ treatment (Fig. 3d, e). Similar results were obtained when the assay was performed in enhanced medium (Extended Data Fig. 6d, e). These results reinforce the view that Cabo and BEZ exert an impact on the PCa tumour microenvironment in part via selective depletion of MDSCs.

As cytokine signalling plays a pivotal role in the recruitment and activation of MDSCs<sup>6</sup>, we further explored the impact of combination treatment on cytokine production in primary CRPC. Cytokine arrays revealed that several key cytokines involved in regulating recruitment and activity of immunosuppressive myeloid cells, including CCL5, CCL12, CD40, and HGF, were reduced by Cabo + ICB or BEZ + ICB treatment. These treatments were also associated with increased IL-1ra, CD142, and VEGF (Fig. 3f and Extended Data Fig. 7a). IL-1ra may contribute to reduced MDSC infiltration<sup>26</sup>. We confirmed that recombinant IL-1ra inhibited IL-1 induced chemoattraction of MDSCs, and this effect was blocked by IL-1ra neutralizing antibody (Fig. 3g). Notably, the cytokine changes were significantly less pronounced in Dasa + ICB treatment (Extended Data Fig. 7b). Noting that cytokine production by cancer cells may influence the functional status of myeloid cells, we cultured MDSCs isolated from CRPC with conditioned medium from the CPPSML PCa cell lines (Extended Data Fig. 7c) and showed upregulated expression of genes responsible for MDSC-induced immune suppression, including *Arg1*, *Cybb*, *Ncf1*, and *Ncf4* (refs 6, 11) (Fig. 3h). Critically, the expression induction was largely abolished if the PCa cells were pre-treated with Cabo or BEZ before conditioned medium was collected (Fig. 3i), whereas direct treatment of MDSCs with Cabo or BEZ caused insignificant expression changes (data not shown), suggesting that certain cytokines in the conditioned

medium may drive the gene upregulation. Through cytokine array (Extended Data Fig. 7d), we identified ten cytokines significantly downregulated in the conditioned medium of PCa cells pre-treated with Cabo or BEZ (Fig. 3j), among which CCL5 was also identified as a downregulated cytokine in Cabo + ICB- and BEZ + ICB-treated CRPC (Fig. 3f). When MDSCs isolated from CRPC tumours were treated with each of the ten cytokines in the presence of Cabo or BEZ, significant upregulation of *Arg1*, *Cybb*, *Ncf1*, and *Ncf4* was observed with most of the cytokines tested (Extended Data Fig. 7e). Therefore, PCa cells are capable of driving immunosuppression-related gene expression in MDSCs through secretion of multiple cytokines, and this paracrine signalling is impaired by Cabo or BEZ treatment.

BEZ targets multiple p110 isoforms. To test whether isoform-specific PI3K inhibitors would generate a comparable level of synergistic advantage when combined with ICB, we tested PI-3065 (p110 $\delta$ -selective inhibitor<sup>27</sup>) and GSK2636771 (p110 $\beta$ -selective inhibitor<sup>28</sup>). Moreover, given the critical role of Cxcr2 in MDSC recruitment<sup>10,11</sup> and the downregulation of Cxcr2 ligands Cxcl1 and Cxcl2 in the conditioned medium of PCa cells treated with Cabo and BEZ (Fig. 3j), we also tested a novel clinical-stage Cxcr1/2 inhibitor SX-682 (Extended Data Fig. 7f, g) as monotherapy or in combination with ICB in the CPPSML model. Mild to moderate effects of PI-3065, GSK2636771, or SX-682 as single agents on CRPC progression were observed, yet combination with ICB produced strong efficacy (Fig. 4a, b). To give further credential to our model and assess the pattern of MDSCs in human PCa, a 32-antibody CyTOF panel was developed (Extended Data Table 1b) and used to analyse 12 fresh fine-needle biopsy samples from ten treatment-naive PCa tumours (Extended Data Table 1c). Analysis with SPADE software displayed the heterogeneous immune cell populations (Extended Data Fig. 8). Results showed the prominence of Gr-MDSCs relative to Mo-MDSCs, with the latter occupying no nodes in the SPADE tree (Fig. 4c). Total T-cell load across

the samples varied considerably (Fig. 4d), yet the frequency of CD8<sup>+</sup> T cells correlated inversely with the frequency of Gr-MDSCs (Fig. 4e), a pattern consistent with the conservation of antagonistic activity of Gr-MDSCs on CD8<sup>+</sup> T cells in human PCA.

Here, by using a chimaeric model of mCRPC, we have shown that ICB alone is insufficient to generate an effective response, but a combination of ICB with drugs that inactivate MDSCs demonstrates superior synergistic efficacy against *de novo* resistance to ICB (Extended Data Fig. 9). The differential sensitivity of MDSCs and CD8<sup>+</sup> T cells to Cabo, BEZ, and possibly other phosphokinase inhibitors should provide an avenue for optimizing the dose and schedule for effective silencing of MDSCs while simultaneously sparing cytotoxic T lymphocytes to attack cancer cells. As with all preclinical model systems and human clinical pathological correlations, prospective clinical trials will be needed to substantiate the hypotheses of our work. Future studies should explore the combination therapy in the context of both established mCRPC and newly diagnosed PCA together with selective anti-androgens to achieve durable clinical response in this major cancer of men.

**Online Content** Methods, along with any additional Extended Data display items and Source Data, are available in the online version of the paper; references unique to these sections appear only in the online paper.

Received 15 November 2016; accepted 31 January 2017.

Published online 20 March 2017.

- Watson, P. A., Arora, V. K. & Sawyers, C. L. Emerging mechanisms of resistance to androgen receptor inhibitors in prostate cancer. *Nature Rev. Cancer* **15**, 701–711 (2015).
- Sharma, P. & Allison, J. P. The future of immune checkpoint therapy. *Science* **348**, 56–61 (2015).
- Kwon, E. D. *et al.* Ipilimumab versus placebo after radiotherapy in patients with metastatic castration-resistant prostate cancer that had progressed after docetaxel chemotherapy (CA184-043): a multicentre, randomised, double-blind, phase 3 trial. *Lancet Oncol.* **15**, 700–712 (2014).
- Beer, T. M. *et al.* Randomized, double-blind, phase III trial of ipilimumab versus placebo in asymptomatic or minimally symptomatic patients with metastatic chemotherapy-naïve castration-resistant prostate cancer. *J. Clin. Oncol.* **35**, 40–47 (2017).
- Topalian, S. L. *et al.* Safety, activity, and immune correlates of anti-PD-1 antibody in cancer. *N. Engl. J. Med.* **366**, 2443–2454 (2012).
- Gabrilovich, D. I. & Nagaraj, S. Myeloid-derived suppressor cells as regulators of the immune system. *Nature Rev. Immunol.* **9**, 162–174 (2009).
- Vuk-Pavlović, S. *et al.* Immunosuppressive CD14<sup>+</sup>HLA-DR<sup>low</sup> monocytes in prostate cancer. *Prostate* **70**, 443–455 (2010).
- Brusa, D. *et al.* Circulating immunosuppressive cells of prostate cancer patients before and after radical prostatectomy: profile comparison. *Int. J. Urol.* **20**, 971–978 (2013).
- Hossain, D. M. *et al.* TLR9-targeted STAT3 silencing abrogates immunosuppressive activity of myeloid-derived suppressor cells from prostate cancer patients. *Clin. Cancer Res.* **21**, 3771–3782 (2015).
- Di Mitri, D. *et al.* Tumour-infiltrating Gr-1<sup>+</sup> myeloid cells antagonize senescence in cancer. *Nature* **515**, 134–137 (2014).
- Wang, G. *et al.* Targeting YAP-dependent MDSC infiltration impairs tumor progression. *Cancer Discov.* **6**, 80–95 (2016).
- Shen, M. M. & Abate-Shen, S. Molecular genetics of prostate cancer: new prospects for old challenges. *Genes Dev.* **24**, 1967–2000 (2010).
- Ding, Z. *et al.* Telomerase reactivation following telomere dysfunction yields murine prostate tumors with bone metastases. *Cell* **148**, 896–907 (2012).
- Ding, Z. *et al.* SMAD4-dependent barrier constrains prostate cancer growth and metastatic progression. *Nature* **470**, 269–273 (2011).
- Araujo, J. C. *et al.* Docetaxel and dasatinib or placebo in men with metastatic castration-resistant prostate cancer (READY): a randomised, double-blind phase 3 trial. *Lancet Oncol.* **14**, 1307–1316 (2013).
- Smith, M. *et al.* Phase III study of cabozantinib in previously treated metastatic castration-resistant prostate cancer: COMET-1. *J. Clin. Oncol.* **34**, 3005–3013 (2016).

- Carver, B. S. *et al.* Reciprocal feedback regulation of PI3K and androgen receptor signaling in PTEN-deficient prostate cancer. *Cancer Cell* **19**, 575–586 (2011).
- Jia, S. *et al.* Opposing effects of androgen deprivation and targeted therapy on prostate cancer prevention. *Cancer Discov.* **3**, 44–51 (2013).
- Peng, W. *et al.* Loss of PTEN promotes resistance to T cell-mediated immunotherapy. *Cancer Discov.* **6**, 202–216 (2016).
- Kim, K. *et al.* Eradication of metastatic mouse cancers resistant to immune checkpoint blockade by suppression of myeloid-derived cells. *Proc. Natl Acad. Sci. USA* **111**, 11774–11779 (2014).
- Rivera, L. B. *et al.* Intratumoral myeloid cells regulate responsiveness and resistance to antiangiogenic therapy. *Cell Reports* **11**, 577–591 (2015).
- De Henau, O. *et al.* Overcoming resistance to checkpoint blockade therapy by targeting PI3K $\gamma$  in myeloid cells. *Nature* **539**, 443–447 (2016).
- Kaneda, M. M. *et al.* PI3K $\gamma$  is a molecular switch that controls immune suppression. *Nature* **539**, 437–442 (2016).
- Frick, A. *et al.* Immune cell-based screening assay for response to anticancer agents: applications in pharmacogenomics. *Pharm. Genomics Pers. Med.* **8**, 81–98 (2015).
- Schade, A. E. *et al.* Dasatinib, a small-molecule protein tyrosine kinase inhibitor, inhibits T-cell activation and proliferation. *Blood* **111**, 1366–1377 (2008).
- Tu, S. *et al.* Overexpression of interleukin-1 $\beta$  induces gastric inflammation and cancer and mobilizes myeloid-derived suppressor cells in mice. *Cancer Cell* **14**, 408–419 (2008).
- Ali, K. *et al.* Inactivation of PI(3)K p110 $\delta$  breaks regulatory T-cell-mediated immune tolerance to cancer. *Nature* **510**, 407–411 (2014).
- Costa, C. *et al.* Measurement of PIP3 levels reveals an unexpected role for p110 $\beta$  in early adaptive responses to p110 $\alpha$ -specific inhibitors in luminal breast cancer. *Cancer Cell* **27**, 97–108 (2015).

**Supplementary Information** is available in the online version of the paper.

**Acknowledgements** We thank N. Feng for advice on preclinical drug dosing; X. Xu and K. O'Connor for technical support on mES cells and chimaera generation; P. Jones and C. Carroll for providing <sup>19</sup>F NMR spectroscopy data; K. Zhao, Z. Xu, and Z. Fang for animal husbandry; F. Giancotti for suggestions on manuscript writing; A. Varma and J. W. Han for technical assistance; G. Wang, E.-J. Jin, P. Dey, and all members of the DePinho laboratory for a variety of technical support and suggestions. The project was supported by U01CA141508 (R.A.D.), P01CA117969 (R.A.D.), Department of Defense Prostate Cancer Research Program (PCRP) Idea Development Award–New Investigator Option W81XWH-14-1-0576 (X.L.), National Institutes of Health grant R44HL072614 (D.Y.M.), and the Clayton & Modesta Williams Cancer Research Fund (R.A.D.). Facility-based experimental support was provided by the Small Animal Imaging Facility (C. Kingsley, V. Tran, K. Maldonado, C. Kaffes), Flow Cytometry and Cellular Imaging Core Facility (J. Burks, D. Mak, and K. Dwyer), and Laboratory Animal Genetic Services (F. Benavides) at The University of Texas MD Anderson Cancer Center (Cancer Center Support Grant P30CA016672).

**Author Contributions** X.L., R.A.D., Y.A.W., and J.W.H. conceived the project and discussed experiments; J.W.H. designed the methodology for, and oversaw, the chimaeric modelling; X.L., E.P., and X.S. acquired and analysed the data; P.D. performed mouse genotyping; X.S., P.D., and Q.C. performed histology staining; P.T. collaborated on providing fresh human samples; S.J. oversaw and performed animal colony management; D.Y.M. provided study drug SX-682 and technical assistance for its use; J.A.Z. suggested MDSC experiments with SX-682 in the model; P.S. provided key suggestions on experiments; Y.A.W. and R.A.D. supervised the research; X.L., R.A.D., Y.A.W., and D.J.S. wrote the manuscript.

**Author Information** Reprints and permissions information is available at [www.nature.com/reprints](http://www.nature.com/reprints). The authors declare no competing financial interests. Readers are welcome to comment on the online version of the paper. Publisher's note: Springer Nature remains neutral with regard to jurisdictional claims in published maps and institutional affiliations. Correspondence and requests for materials should be addressed to R.A.D. ([rdepinho@mdanderson.org](mailto:rdepinho@mdanderson.org)) or Y.A.W. ([yalanwang@mdanderson.org](mailto:yalanwang@mdanderson.org)).

**Reviewer Information** *Nature* thanks D. Gabrilovich, M. Galsky, R. Madan and the other anonymous reviewer(s) for their contribution to the peer review of this work.

## METHODS

**Ethics statement and transgenic mice.** All animal work performed in this study was approved by The University of Texas MD Anderson Cancer Center Institutional Animal Care and Use Committee. All animals were maintained in pathogen-free conditions and cared for in accordance with the International Association for Assessment and Accreditation of Laboratory Animal Care policies and certification. All surgeries were performed with isoflurane anaesthesia. Analgesic was administered after surgery along with temperature-controlled post-surgical monitoring to minimize suffering. *PB-Cre<sup>+</sup> Pten<sup>L/L</sup> p53<sup>L/L</sup> Smad4<sup>L/L</sup>* mice were described previously<sup>13</sup>. Mice were crossed to *Rosa26-Lox-tdTomato-Lox-EGFP (mTmG) allele<sup>29</sup>* (The Jackson Laboratory, 007676) and *Rosa26-pCAGGS-LSL-luciferase (LSL-LUC) allele* (MMRRC, 01XAC), both of which were already congenic to C57BL/6, and further backcrossed to C57BL/6 background for four generations. Mice were then intercrossed to obtain 'CPPSML' males with homozygous status of *Pten*, *p53*, and *Smad4*, heterozygous status of *mTmG* and *LSL-LUC*, and hemizygous status of *PB-Cre*. To calculate the expected frequency of pups to develop prostate tumours, several factors were included: only males were considered; *PB-Cre* had to be transmitted from males to the next generation owing to the non-specific expression in oocytes<sup>30</sup>, thus only half of the litter was *Cre<sup>+</sup>*; moreover, to circumvent paternal infertility caused by the diseased prostate, the key loxP-flanked tumour suppressor alleles (for example, *Pten/p53* (ref. 31), or *Pten/Smad4* (ref. 14)) that were needed for aggressive PCa were maintained as heterozygous state for the *Pten* loxP allele in the males for continued fertility (*p53* or *Smad4* could be homozygous)<sup>13,14</sup>, thus only half of the litter was homozygous for all tumour suppressor alleles. Mice with spontaneous prostate tumours were euthanized at designated time points for tumour collection. Owing to the internal status of the tumours, we used signs of lethargy, reduced mobility, and morbidity, rather than maximal tumour size, as a protocol-enforced end point.

**mES cell derivation.** *Pten<sup>L/L</sup> p53<sup>L/L</sup> Smad4<sup>L/L</sup> mTmG<sup>L/L</sup>* or *Pten<sup>L/L</sup> p53<sup>L/L</sup> Smad4<sup>L/L</sup> LSL-LUC<sup>L/L</sup>* female mice 3–4 weeks old were administered 5 international units (IU) of pregnant mare serum gonadotropin (NHPP: National Hormone & Peptide Program) by intraperitoneal injection at 15:00–16:00. Females were then administered 5 IU of human chorionic gonadotropin (Sigma-Aldrich, C1063) by intraperitoneal injection 46 h after pregnant mare serum gonadotropin and mated 1:1 with *PB-Cre<sup>+</sup> Pten<sup>L/L</sup> p53<sup>L/L</sup> Smad4<sup>L/L</sup> LSL-LUC<sup>L/L</sup>* or *PB-Cre<sup>+</sup> Pten<sup>L/L</sup> p53<sup>L/L</sup> Smad4<sup>L/L</sup> mTmG<sup>L/L</sup>* male mice, respectively. Successful mating was evaluated and noted by presence of copulus plug 14–16 h after mating. Blastocyst-stage embryos were isolated from those plugged females at embryonic day 3.5 by uterine isolation and flush. Blastocysts were collected and cultured on 16 h pre-plated inactivated mouse embryonic fibroblasts in pre-equilibrated mES cell culture media. Culture media included knockout serum replacement (Invitrogen, 10828010), knockout DMEM (Invitrogen, 10829-018), GlutaMAX (Invitrogen, 35050079), sodium pyruvate (Invitrogen, 11360-070), non-essential amino acids (Invitrogen, 11140050), 2-mercaptoethanol (Invitrogen, 21985-023), penicillin–streptomycin (Invitrogen, 15140-122), insulin (Sigma-Aldrich, 12643), LIF (Millipore, ESG1107), mitogen-activated inhibitor (Stemgent, PD0325901), and glycogen synthase kinase inhibitor (Stemgent, CHIR99021). All components were prepared and filter sterilized before use. The culture dish containing the isolated blastocysts was left undisturbed in a water-jacketed copper-shelved incubator at 37 °C and 5% CO<sub>2</sub>. Six days after isolation and culture, mES cell outgrowths were visible and individually picked using an Oxford P20 pipette with sterile 100 µl round gel filtered tips (USA Scientific, 1022-0810). Each outgrowth was transferred to a well of a sterile 96-well U-bottomed dish containing 15 µl sterile PBS. Forty-five microlitres of 0.25% trypsin-EDTA (Invitrogen, 25200-056) was added to each well. After incubation for 4 min at 37 °C with 5% CO<sub>2</sub>, each well was quenched with 300 µl of mES cell media containing fetal bovine serum (FBS) and pipetted up and down six to eight times using a multichannel pipette with sterile elongated tips, to generate cell clumps. Individual cell clump populations were transferred to corresponding wells of a 48-well plate containing 14–16 h pre-plated mouse embryonic fibroblasts in pre-equilibrated mES cell culture medium. Once the wells reached ~80% confluency they were split to triplicate plates for expansion in culture, freezing, and DNA isolation. Generated mES cell lines were genotyped and clones with the genotype *PB-Cre<sup>+</sup> Pten<sup>L/L</sup> p53<sup>L/L</sup> Smad4<sup>L/L</sup> mTmG<sup>L/L</sup> LSL-LUC<sup>L/L</sup>* (CPPSML) were selected. They were confirmed to be mycoplasma negative, and screened for the presence of the Y chromosome. Chromosome spreads were prepared and observed for abnormalities. Background characterization was performed by single-nucleotide polymorphism analysis.

**Chimaera cohort development.** Derived mES cell lines JH58 and JH61 were genotyped as *PB-Cre<sup>+</sup> Pten<sup>L/L</sup> p53<sup>L/L</sup> Smad4<sup>L/L</sup> mTmG<sup>L/L</sup> LSL-LUC<sup>L/L</sup>* (CPPSML) and confirmed to contain the Y chromosome. Chimaera cohorts were produced by blastocyst microinjection of the mES cells into C57BL/6N-Tac-Tyr<sup>tm1Arte</sup> (Taconic, 11971) then followed by uterine implantation into pseudo-pregnant CD-1 (Charles River, 022) or Swiss Webster (Taconic, SW-F) female mice.

Specifically, cell lines were cultured to roughly 80% confluence on inactivated mouse embryonic fibroblasts in wells of a 24-well plate in mES cell culture media described above. Cells cultured for injection were split 11–16 h before preparation for microinjection. Cells were removed from incubation, washed with sterile PBS, and trypsinized with 0.25% trypsin-EDTA. Trypsin was quenched with mES cell culture media containing FBS and the cell culture plate was returned to incubation for 45 min to allow the larger mouse embryonic fibroblasts to re-attach to the bottom of the cell culture well. After that incubation, the desired mES cells were collected and transferred to a 15 ml conical tube. The suspension was brought up to 5 ml with mES cell culture media, gently pipetted up and down to mix, and then spun down at 4 °C and 800 r.p.m. for 4 min. All except 100–200 µl of media was aspirated from the tube. The bottom of the conical tube was tapped externally to break up the cell pellet and the tube was placed on ice for microinjection use.

C57BL/6N-Tac-Tyr<sup>tm1Arte</sup> female mice that had achieved successful strain-matched mating after superovulation via timed gonadotropin administration were used as donors for 3.5 day blastocysts. Blastocysts were collected by uterine flush and cultured in M16 medium (Millipore, MR-016-D) overlaid with embryo-tested oil in a 35 mm culture dish at 37 °C with 5% CO<sub>2</sub>. Blastocysts were each micro-manipulated to insert roughly 12 individual mES cells into its blastocoel. Injected blastocysts were then implanted into the uteri of pseudo-pregnant females. Each pseudo-pregnant female received up to 14 micromanipulated blastocysts (up to seven blastocysts per uterine horn). Chimaeras were verified with prostate tumour formation by MRI and assigned into preclinical studies through randomization which maximized the chance that male mice housed in the same cage received different drugs. Blinding was not applied, because allocation required investigators to assess mouse prostate tumour size with MRI before randomization. Pups were excluded from tumour analysis if they died without significant sign of tumour formation.

**Single-nucleotide polymorphism analysis.** Single-nucleotide polymorphism analysis was performed in the Genetic Services core at MD Anderson Cancer Center. For background characterization of the JH61 ES cell line, 80 microsatellite (simple sequence length polymorphism, SSLP) markers, polymorphic between FVB/N and 129S6 inbred strains, and evenly distributed along the genome (that is, genome scan), were used as described<sup>32</sup>. To analyse the MHC region on mouse chromosome 17, an extra 15 polymorphic SSLPs flanking the H2 complex were added. The results (allele type) obtained for the SSLP in the H2 region were confirmed by means of H2 polymerase chain reaction–restriction fragment length polymorphism (PCR-RFLP) genotype as described<sup>33</sup>.

**Non-invasive mouse and ex vivo imaging.** For MRI imaging with Bruker ICON, the animals were anaesthetized with 1–3% isoflurane and placed on the ICON animal bed. The MRI coil was secured into position over the animal and the entire bed assembly was placed into the Bruker ICON 1T MRI bore. Rapid acquisition with relaxation enhancement (RARE) T2-weighted images were acquired in both the coronal and axial planes. After the imaging was completed, the animals were allowed to recover under a heating lamp until fully conscious. MRI images were loaded into ImageJ to manually demarcate the contour of the prostate and calculate the total volume. Bioluminescence imaging with IVIS Spectrum was performed as previously described<sup>34</sup>. Fluorescence imaging of dissected prostate tumours, the pair of draining lymph nodes, and lung was performed with a Leica M165FC fluorescence stereomicroscope. Lymph node metastasis score was assigned as 0 (no GFP<sup>+</sup> tumour cells), 1 (sparse GFP<sup>+</sup> tumour cells on one lymph node), 2 (sparse GFP<sup>+</sup> tumour cells on both lymph nodes, or strong GFP<sup>+</sup> tumour cell patches on only one lymph node), 3 (sparse GFP<sup>+</sup> tumour cells on one lymph node and strong GFP<sup>+</sup> tumour cell patches on the other lymph node), or 4 (strong GFP<sup>+</sup> tumour cell patches on the both lymph nodes). Spontaneous lung micrometastasis was quantified by counting tumour cell clusters with more than ten GFP<sup>+</sup> tumour cells in each cluster.

**Immunohistochemistry, immunofluorescence, and western blot.** Tissues were fixed in 10% formalin overnight and embedded in paraffin. Immunohistochemical and immunofluorescence staining was performed as previously described<sup>11,14</sup>. Immunohistochemical slides were scanned with a Panoramic Digital Slide Scanner (3DHISTECH) and images were cropped from virtual slides in Panoramic Viewer. Immunofluorescence slides were imaged with a Nikon A1R Confocal Laser Microscope and quantified with ImageJ. Primary antibodies used included CK5 (Covance, PRB-160P), CK8 (Covance, MMS-162P), Ki67 (Fisher, RM-9106-S1), cleaved caspase 3 (Cell Signaling Technology, 9661), Gr-1 (BioLegend, 108401), phospho-S6 (Cell Signaling Technology, 4858). For western blot analysis, cells or fresh tissues were lysed on ice using RIPA buffer (Boston BioProducts) supplemented with protease and phosphatase inhibitors (Roche). Western blot procedure was performed as previously described<sup>11,14</sup>. Primary antibodies used included phospho-Met (Cell Signaling Technology, 3077), phospho-VEGFR2 (Cell Signaling Technology, 3770), phospho-Erk1/2 (Cell Signaling Technology, 4370), phospho-Akt (Cell Signaling Technology, 4060),

phospho-mTOR (Cell Signaling Technology, 5536), phospho-p70 S6K (Cell Signaling Technology, 9234), phospho-S6 (Cell Signaling Technology, 4856), and vinculin (Millipore, 05-386).

**Targeted pathway inhibitors.** Enzalutamide (MedKoo Biosciences, 201821) was admixed with Purina 5053 Chow at 50 mg of drug per kilogram of diet (Research Diets), which, when fed to mice, could reach approximately 10 mg per kg per day dose<sup>35</sup> (calculation based on average body mass of 25 g and daily food intake of 5 g per day, with online calculator at [www.researchdiets.com/resource-center-page/diet-dose-calculator](http://www.researchdiets.com/resource-center-page/diet-dose-calculator)). To induce castration-resistant PCa, mice with prostate tumour confirmed by MRI were surgically castrated and started on an Enzalutamide diet for 3 weeks before being moved back to regular chow and treated with therapeutic drugs. For *in vivo* pharmacological inhibition, BEZ235 (Selleck Chemicals, S1009), cabozantinib (Selleck Chemicals, S1119), dasatinib (Selleck Chemicals, S1021), PI-3065 (MedKoo, 407192), and GSK2636771 (MedKoo, 205844) were orally administered at daily doses of 45 mg per kg, 30 mg per kg, 30 mg per kg, 50 mg per kg, and 30 mg per kg, respectively, daily on a Monday–Friday schedule. SX-682 (Syntrix Biosystems) was orally administered twice a day at 50 mg per kg actual dose on a Monday–Friday schedule. Similar drug dosing methods were described previously<sup>27,28,36–38</sup>. The doses we used for cabozantinib and BEZ235 are clinically relevant: for cabozantinib, to convert the mouse dose into human dose, we calculated  $30 \text{ mg per kg} \times (1/12.3) = 2.4 \text{ mg per kg}$  daily in human (the conversion factor 12.3 can be found in FDA guidance at <http://www.fda.gov/downloads/Drugs/.../Guidances/UCM078932> and in ref. 39). Given a typical human weight of 60 kg, the clinical dose range of 60 mg daily (PCa, renal cell carcinoma) to 140 mg daily (medullary thyroid cancer) converts to a human dose range of 1–2.3 mg per kg daily. Therefore, our cabozantinib dose in mice approximates the approved dose for treating medullary thyroid cancer, and is 1.4 times higher than used in COMET-1 and COMET-2 phase III trials of advanced PCa. For BEZ235, previous studies showed that while 300 or 400 mg twice daily<sup>40</sup> showed significant toxicity in patients, 200 mg twice daily displayed higher tolerability<sup>41</sup>. The dose we used in the mice study, 45 mg per kg daily, is approximately equivalent to 225 mg daily in humans, and thus is within range of tolerable clinical doses. For ICB and Gr1-neutralizing antibody treatment, anti-PD1 (clone RMP1-14, BioXcell, BE0146), anti-CTLA4 (clone 9H10, BioXcell, BE0131), or anti-Gr1 (clone RB6-8C5, BioXcell, BE0075) antibodies (or their respective isotype IgG controls) were intraperitoneally administered at 200 µg per injection three times per week. The duration of drug treatment was typically 4 weeks before endpoint analysis.

**CyTOF of human specimens and mouse tumours.** CyTOF analysis of mouse prostate tumours with data analysed in FlowJo (Tree Star) followed our previous methods<sup>11</sup>. Human prostate fine-needle aspirate specimens were acquired under approved institutional review board Protocol PA14-0420 at MD Anderson Cancer Center. Informed consent was obtained from all subjects. Prostate tumour single cells were isolated using a Human Tumour Dissociation kit (Miltenyl Biotec, 130-095-929). All isolated cells were depleted of erythrocytes by hypotonic lysis. Cells were blocked with FcR Blocking Reagent (Miltenyl Biotec, 130-059-901) for 10 min and incubated with CyTOF antibody mix for 30 min at room temperature. Cells were washed once and incubated with Cell-ID Cisplatin (Fluidigm, 201064) at 2.5 µM for 2.5 min for viability staining. Cells were fixed with MaxPar Fix and Perm Buffer containing Cell-ID Intercalator-Ir (Fluidigm, 201192A) at 0.125 µM and 4 °C overnight to stain the nuclei. The samples were analysed with a CyTOF instrument (Fluidigm) in the Flow Cytometry and Cellular Imaging Core Facility at MD Anderson Cancer Center. Data were analysed with FlowJo (Tree Star) and SPADE software<sup>42</sup>.

**Cell isolation and *in vitro* survival and migration assay.** Over 95% of all CD11b<sup>+</sup>Gr1<sup>+</sup> myeloid cells in established naive or castration-resistant prostate tumours in CPPSML mice are granulocytic (Ly-6G<sup>+</sup> Ly-6C<sup>low</sup>), similar to the level in the *PB-Cre<sup>+</sup> Pten<sup>L/L</sup> Smad4<sup>L/L</sup>* model that we recently reported<sup>11</sup>. Gr-MDSCs were isolated from prostate tumours by first enriching for lymphocytes using Lympholyte-M Cell Separation Media (Cederlane, CL5031) followed by MACS-based isolation using a Mouse MDSC Isolation Kit (Miltenyl Biotec, 130-094-538) and plated in RPMI1640 supplemented with 10% FBS and antibiotics. From the same mice, CD8<sup>+</sup> T cells were isolated from the spleen using a Mouse CD8a<sup>+</sup> T Cell Isolation Kit (Miltenyl Biotec, 130-104-075). MDSCs and CD8<sup>+</sup> T cells were cultured as described<sup>20</sup>. GFP<sup>+</sup> PCa cells were isolated from the prostate tumours by fluorescence-activated cell sorting with a BD FACSAria III Cell Sorter, and cultured in complete DMEM supplemented with 10% FBS and antibiotics. The purity of Gr-MDSCs (CD11b<sup>+</sup>Gr1<sup>+</sup>Ly6G<sup>+</sup>Ly6C<sup>low</sup>F4/80<sup>-</sup>), CD8<sup>+</sup> T-cell (CD3<sup>+</sup>CD8<sup>+</sup>), and PCa-cell (GFP<sup>+</sup>Tomato<sup>-</sup>CD45<sup>-</sup>) populations was greater than 90%, as determined by flow cytometry. A survival assay was performed on 96-well plates with Cell Proliferation Reagent WST-1 (Sigma-Aldrich, 11644807001) as described<sup>20</sup>. Serially diluted drugs (BEZ, Cabo, Dasa) were added to the culture to construct dose–response curves and the IC<sub>50</sub> value was calculated with GraphPad Prism 6 software. For the migration assay, Gr-MDSCs isolated from prostate tumours

using MACS technology were added to the upper chamber of a 24-well trans-well system (BD Falcon). MDSC short-term culture medium (RPMI1640 supplemented with 10% FBS) with the indicated concentrations of recombinant mouse IL-1α (BioLegend, 575002), IL-1β (BioLegend, 575102), IL-1ra (VWR, 10006-448), or mouse IL-1ra neutralizing antibody (R&D Systems, AF-480-NA) was added to the bottom chamber. Cells were allowed to migrate to the bottom well for 6 h at 37 °C with 5% CO<sub>2</sub>. Migrated cells were fixed and stained with crystal violet for quantification.

**T-cell suppression assay and quantification of cytokine production.** A T-cell suppression assay was performed as we previously described<sup>11</sup> using equal numbers of MACS-sorted intratumoural Gr-MDSCs and CFSE- (Invitrogen) labelled MACS-sorted CD8<sup>+</sup> or CD4<sup>+</sup> T cells from spleen of wild-type C57BL/6 mice (The Jackson Laboratory, 000664). To assess the effect of drugs (BEZ, Cabo, Dasa) on the proliferation of T cells, drugs at different concentrations were added to anti-CD3/anti-CD28-stimulated CFSE-labelled and MACS-sorted CD8<sup>+</sup> or CD4<sup>+</sup> T cells from spleen of wild-type C57BL/6 mice at time zero. CFSE intensity was quantified 72 h later with peaks identified by a BD LSRFortessa Cell Analyzer. CFSE peaks indicated the division times. Division times 0, 1–2, and ≥3 were defined as no proliferation, moderate proliferation, and high proliferation, respectively. Viable CD4<sup>+</sup> or CD8<sup>+</sup> T cells (viability defined as negative DAPI (4',6-diamidino-2-phenylindole) stain) falling in each category were quantified as the percentage of total live CD4<sup>+</sup> or CD8<sup>+</sup> T cells, respectively. The supernatant medium was used to quantify IFNγ and IL-2 production by ELISA following the manufacturer's manual (BioLegend, 430804 and 431004).

**Antibody array.** Mouse prostate tumours treated with defined agents were processed as instructed by the manufacturer's protocol, and an equal amount (micrograms) of lysate was used to quantify phospho-RTK proteins with a Proteome Profiler Mouse Phospho-RTK Array Kit (R&D Systems, ARY014) or a Proteome Profiler Mouse XL Cytokine Array Kit (R&D Systems, ARY028). Medium conditioned by CPPSML PCa cell lines was analysed with a Proteome Profiler Mouse Cytokine Array Kit - Panel A (R&D Systems, ARY006). Quantification of the spot intensity in the arrays was conducted with background subtraction in ImageJ.

**Transfection of recombinant proteins.** MACS-sorted MDSCs isolated from mouse prostate tumours were co-transfected with recombinant active ERK2 (R&D Systems, 1230-KS-010) and p70S6K (R&D Systems, 896-KS-010) following the manufacturer's protocol of Chariot Protein Delivery Reagent (Active Motif, 30025). The transfection efficiency was verified to be over 80% in separate wells of MDSCs transfected with β-galactosidase and stained with a Beta-Galactosidase Staining Kit (Clontech, 631780). The effect of co-transfection on the resistance of MDSCs to drug treatment was evaluated 12 h after transfection with Cell Proliferation Reagent WST-1 (Sigma-Aldrich, 11644807001).

**Treatment of MDSCs with PCa-cell conditioned medium.** CPPSML PCa cell lines established and grown in complete DMEM supplemented with 10% FBS were cultured to 90% confluence and renewed with fresh medium followed by medium collection (0.45 µm filtered) 12 h later. The homozygous deletion of *Pten*, *p53*, and *Smad4* was confirmed with genotyping, and all cell lines were confirmed free of mycoplasma with a MycoAlert Mycoplasma Detection Kit (Lonza). When the cells were required to be pre-treated with Cabo or BEZ, the renewed medium was supplemented with the drugs at indicated concentration and added to cells. Twelve hours later, conditioned medium was collected with any floating cells removed by 0.45 µm filter, and subsequently concentrated 50-fold with an Amicon Ultra-15 Centrifugal Filter Unit with Ultracel-3 membrane (Millipore, UFC900324) to deplete small compounds but retain proteins larger than 3 kDa (including most cytokines). Such concentrated medium was diluted back to onefold with complete DMEM. The conditioned medium was used within 12 h of collection to culture MACS-sorted MDSCs isolated from mouse prostate tumours. Unconditioned complete DMEM supplemented with 10% FBS was used as negative control. To test whether supplementing drug pre-treated conditioned medium with specific cytokines could reverse the effect on MDSCs, the ten cytokines (all from BioLegend) were added individually at 100 ng ml<sup>-1</sup>.

**Quantitative RT-PCR.** RNA was isolated by RNeasy Kit (Qiagen) and reversed transcribed using a Superscript III cDNA synthesis Kit (Life Technology). Quantitative PCR was performed using a SYBR-GreenER Kit (Life Technology). The following primers were used: Arg1\_F, CTCCAAGCCAAAGTCCCTTAGAG; Arg1\_R, AGGAGCTGTCATTAGGGACATC; Ncf1\_F, ACACCTTCATTGCGCCATATTGC; Ncf1\_R, TCGGTGAATTTCTGTAGACCAC; Ncf4\_F, GTGAACCTGGCCTGGATCTG; Ncf4\_R, AAGCTGCTCAAAGTCGCTCT; Cybb\_F, CCTCTACAAAACCATTCGGAG; Cybb\_R, CTGTCCACGTACAATTCGTTCA; internal control Gapdh\_F, AGGTCGGTGTGAACGGATTG; Gapdh\_R, TGTAGACCATGTAGTTGAGGTC.

**Preparation of SX-682.** SX-682 synthesis was performed at Syntrix Biosystems and is described in the patent US 8969365 B2 (publication date 3 March 2015).

General chemicals, reagents, and precursors for synthesis were purchased from Sigma-Aldrich (Milwaukee, Wisconsin, USA), Boron Molecular (Research Triangle Park, North Carolina, USA), and Frontier Scientific (Logan, Utah, USA). Solvents were purchased from either VWR International (West Chester, Pennsylvania, USA) or Sigma-Aldrich (Milwaukee, Wisconsin, USA) and used without further purification. The synthesis steps are described below as illustrated in Extended Data Fig. 7g.

2-Chloro-pyrimidine-5-carboxylic acid (**1**) (3.16 g, 20 mmol, Frontier Scientific, Logan, Utah, USA) was suspended in dichloromethane (40 ml), and oxalyl chloride (3.30 g, 26 mmol) was added, followed by DMF (three drops) as catalyst. The reaction started to vigorously evolve gas. The reaction was heated to reflux for 1 h, and then allowed to cool to room temperature. 4-Fluoroaniline (2.44 g, 2.2 mmol) was added, vigorous bubbling was seen again, and the reaction mixture warmed up considerably. Triethylamine (4.05 g, 40 mmol) was added, and a flocculent precipitate immediately formed. The reaction mixture was heated to reflux once again for another hour, removed from heat, and stirred at room temperature for 18 h under nitrogen. The reaction was diluted with EtOAc (100 ml), and the organic layer washed with H<sub>2</sub>O, saturated NaHCO<sub>3</sub>, H<sub>2</sub>O, 1 N HCl, H<sub>2</sub>O, brine, then dried over Na<sub>2</sub>SO<sub>4</sub>. The liquid was filtered, and evaporated to yield 3.44 g (68%) of the 2-chloro-pyrimidine-5-carboxylic acid (4-fluoro-phenyl)-amide as a light yellow solid. Electrospray ionization–mass spectrometry (ESI–MS) (*m/z*): [M]<sup>+</sup> = 252.0. This intermediate was carried forward without further purification.

In a round-bottomed flask, the intermediate 2-chloro-pyrimidine-5-carboxylic acid (4-fluoro-phenyl)-amide (2.52 g, 10.0 mmol) and anhydrous sodium hydrogen sulfide (1.22 g, 21.8 mmol) were suspended in anhydrous DMF (20 ml). The suspension was stirred at room temperature, and the reaction mixture turned a deep green colour. After 1 h, the reaction mixture was partitioned between EtOAc and H<sub>2</sub>O, and transferred to a separatory funnel. After the layers were separated, the organic layer was washed twice with a 2:1 mixture of H<sub>2</sub>O and 5% aqueous NaHCO<sub>3</sub>. The combined aqueous layers were acidified with 1 N HCl precipitating a yellow solid. The suspension was left to stand at room temperature for 2 h, and then the precipitate was collected by vacuum filtration, and rinsed with water. The yellow solid was dried overnight in a vacuum desiccator to yield 2.3 g (92%) of the thiopyrimidinamide intermediate **2**. <sup>1</sup>H NMR (300 MHz, DMSO-*d*<sub>6</sub>) δ 10.29 (s, 1H), 8.77 (bs, 2H), 7.77–7.70 (m, 2H), 7.24 (t, *J* = 8.9 Hz, 2H); ESI–MS (*m/z*): [M]<sup>+</sup> = 250.0.

2-Mercapto-pyrimidine-5-carboxylic acid (4-fluoro-phenyl)-amide intermediate **2** (2.32 g, 9.3 mmol) and 2-bromomethyl-4-trifluoromethoxy-phenylboronic acid, pinacol ester (3.85 g, 10.1 mmol, Boron Molecular, Raleigh, North Carolina, USA) were suspended in anhydrous DMF (20 ml). Sonication was used to dissolve the compounds. To the reaction flask triethylamine (2.8 ml, 20.1 mmol, Sigma Aldrich, Milwaukee, Wisconsin, USA) was added and a precipitate (triethylamine-HBr) immediately formed. The reaction was layered with nitrogen gas and left to stand at room temperature for 3.75 h. The reaction was poured into H<sub>2</sub>O (500 ml) and layered with EtOAc. The biphasic solution was transferred to a separatory funnel and diluted further with EtOAc and brine. The layers were separated, and the aqueous layer was extracted twice more with EtOAc. The combined organic layers were dried over Na<sub>2</sub>SO<sub>4</sub>, gravity filtered, and dried by rotary evaporation to yield 5.7 g (98%) of an oil, 2-[2-(4,4,5,5-tetramethyl-[1,3,2]dioxaborolan-2-yl)-5-trifluoromethoxy-benzylsulfanyl]-pyrimidine-5-carboxylic acid (4-fluoro-phenyl)-amide (**3**). <sup>1</sup>H NMR (500 MHz, DMSO-*d*<sub>6</sub>) δ 10.52 (s, 1H), 9.11 (s, 2H), 7.81 (d, *J* = 8.2 Hz, 1H), 7.78–7.75 (m, 2H), 7.55 (s, 1H), 7.28–7.22 (m, 3H), 4.72 (s, 2H), 1.32 (s, 12H); ESI–MS (*m/z*): [M]<sup>+</sup> = 550.1. The NMR spectrum also contained peaks consistent with the presence of residual DMF. The intermediate was carried forward without further purification.

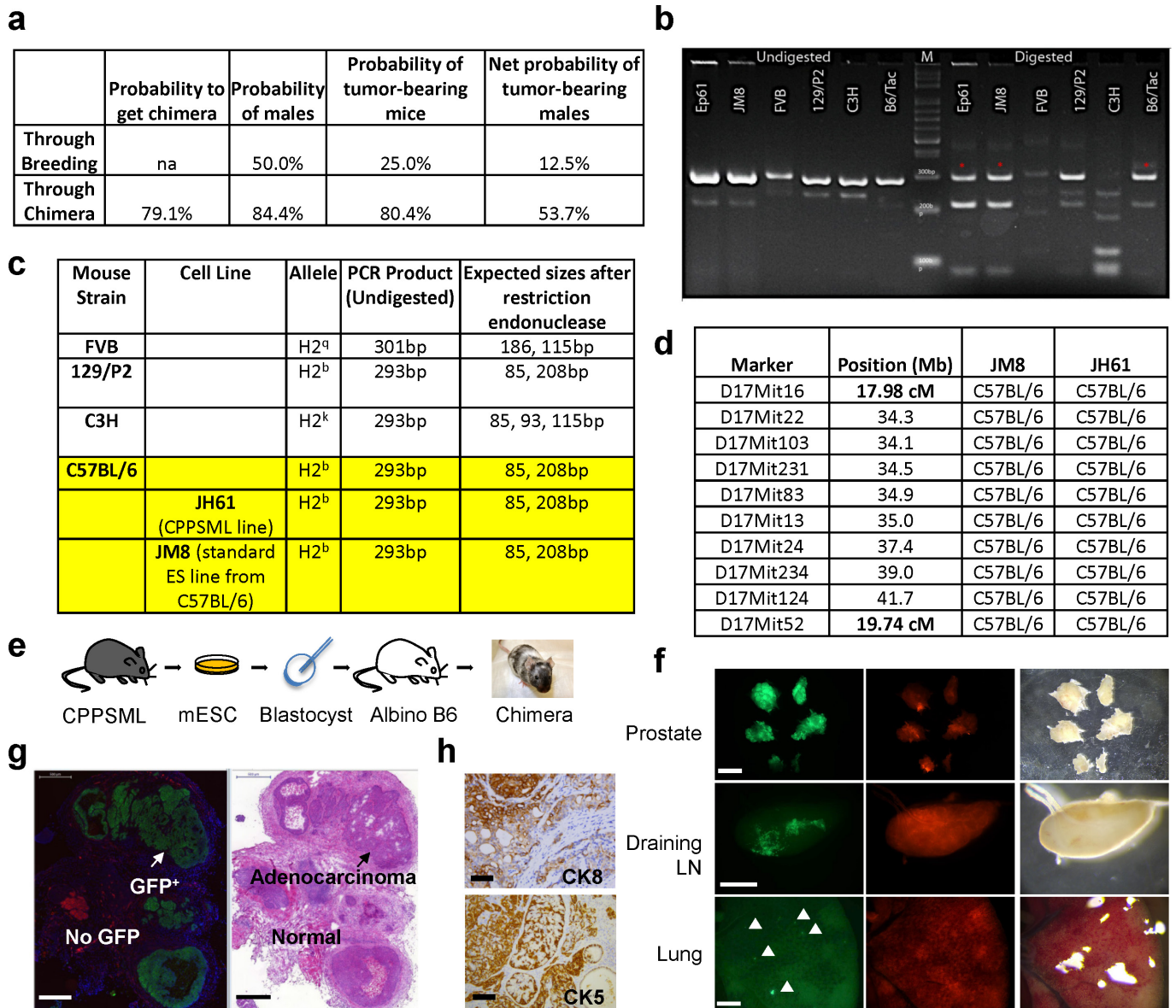
The pinacolyl boronate ester was deprotected via hydrolysis of the intermediate trifluoroborate<sup>43</sup>. Compound **3** (5.66 g, 10.3 mmol, 1 eq.) was dissolved in methanol (100 ml). The reaction vessel was charged with 4.5 M aqueous potassium hydrogen fluoride (11.5 ml, 5 eq.) and the resulting solution was stirred for 1 h. The methanol was removed by rotary evaporation at room temperature and the resulting mixture of yellow and off-white solids was suspended in acetone. The

suspension was gravity filtered to remove the insoluble salts, and the resulting clear yellow solution was added via pipette to a flask of H<sub>2</sub>O (2 l) and placed in the refrigerator. After cooling for about 1.5 h, the resulting off-white precipitate was collected by vacuum filtration, rinsing with water. The funnel was dried overnight in a vacuum desiccator to afford 3.87 g (80%) of 2-(2-boronic acid-5-trifluoromethoxy-benzylsulfanyl)-pyrimidine-5-carboxylic acid (4-fluoro-phenyl)-amide (**4**) (SX-682). Melting point = 211–214 °C; <sup>1</sup>H NMR (300 MHz, DMSO-*d*<sub>6</sub>) δ 10.49 (s, 1H), 9.09 (s, 2H), 8.33 (bs, 2H), 7.78–7.73 (m, 2H), 7.66 (d, *J* = 8.5 Hz, 1H), 7.46 (s, 1H), 7.25–7.19 (m, 3H), 4.70 (s, 2H); <sup>13</sup>C NMR (100.6 MHz, DMSO-*d*<sub>6</sub>) δ 173.7, 161.9, 159.8, 157.4, 156.8, 148.8, 144.7, 136.0, 135.7, 135.0, 123.8, 122.3, 122.2, 121.7, 121.4, 118.8, 118.3, 115.5, 115.3, 34.3; <sup>19</sup>F NMR (300 MHz, DMSO-*d*<sub>6</sub>) δ –56.5 (3F), –118.2 (1F); <sup>11</sup>B NMR (128.4 MHz, DMSO-*d*<sub>6</sub>) δ 21.7; HRMS (*m/z*): [M]<sup>+</sup> calculated for C<sub>19</sub>H<sub>15</sub>BF<sub>4</sub>N<sub>3</sub>O<sub>4</sub>S, 468.0807; found, 468.0803; analysis (calculated, found for C<sub>19</sub>H<sub>14</sub>BF<sub>4</sub>N<sub>3</sub>O<sub>4</sub>S): C (48.84, 48.91), H (3.02, 3.20), N (8.99, 8.99), S (6.86, 6.73).

**Statistical analysis.** Data are presented as mean ± s.d. unless indicated otherwise. Sample size was chosen to ensure 80% power to detect significant effect size on the basis of our recent publications using the transgenic PCa mouse models and thereof derived primary tumour and myeloid cells<sup>11,13,14</sup>. A Student's *t*-test assuming two-tailed distributions or a non-parametric Mann–Whitney *U*-test was used to calculate statistical significance between groups (no assumption was made that variance was similar between the groups being statistically compared). *P* < 0.05 was considered statistically significant.

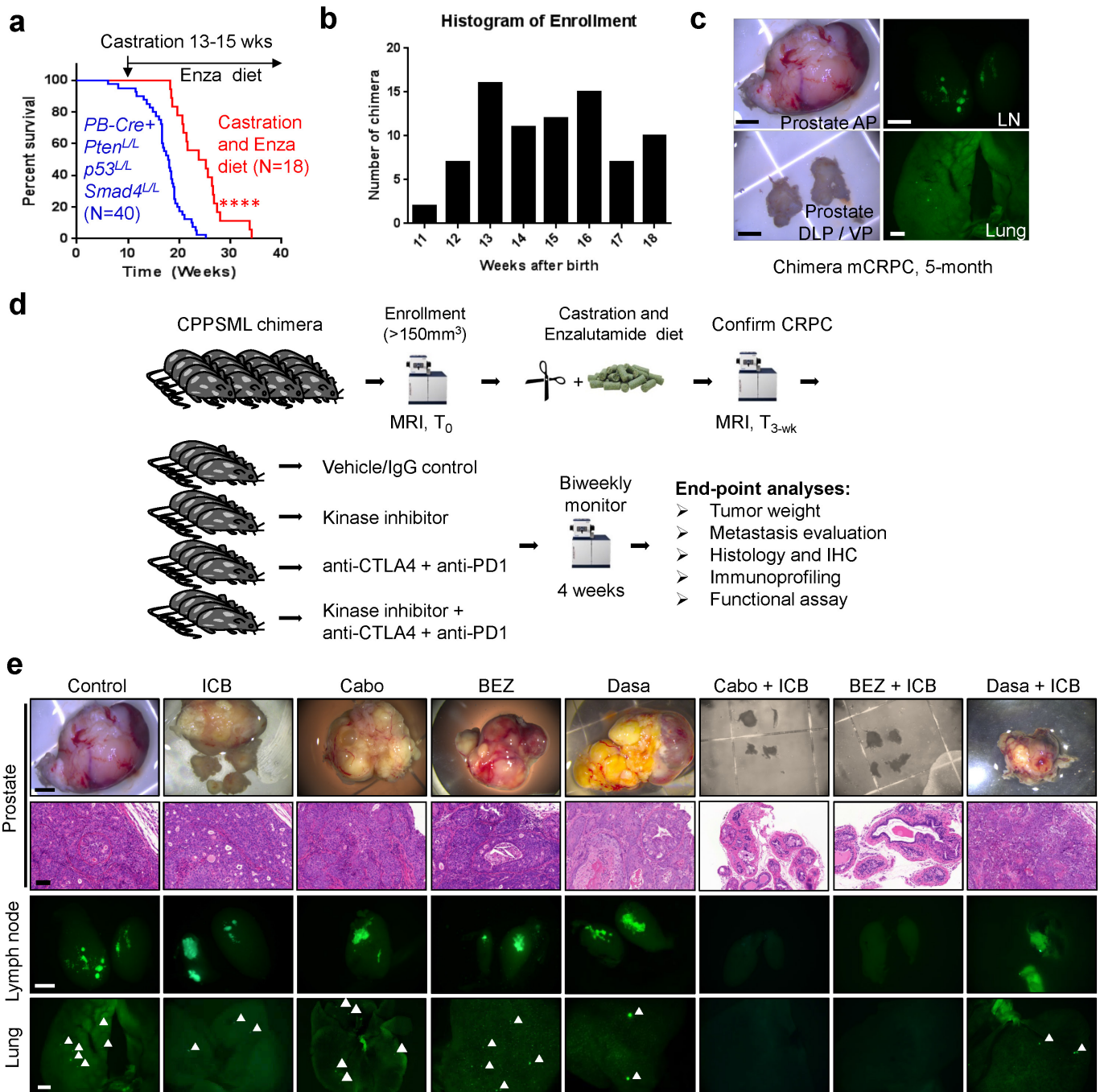
**Data availability statement.** Source Data for the main and Extended Data Figures are provided in the online version of this paper. All other data are available from the corresponding authors upon reasonable request.

- Muzumdar, M. D., Tasic, B., Miyamichi, K., Li, L. & Luo, L. A global double-fluorescent Cre reporter mouse. *Genesis* **45**, 593–605 (2007).
- Birbach, A. Use of PB-Cre4 mice for mosaic gene deletion. *PLoS ONE* **8**, e53501 (2013).
- Chen, Z. *et al.* Crucial role of p53-dependent cellular senescence in suppression of Pten-deficient tumorigenesis. *Nature* **436**, 725–730 (2005).
- Benavides, F. *et al.* Microsatellite DNA variants between the inbred SENCAR mouse strains. *Mol. Carcinog.* **28**, 191–195 (2000).
- Saha, B. K. Typing of murine major histocompatibility complex with a microsatellite in the class II E<sub>b</sub> gene. *J. Immunol. Methods* **194**, 77–83 (1996).
- Lu, X. *et al.* VCAM-1 promotes osteolytic expansion of indolent bone micrometastasis of breast cancer by engaging α4β1-positive osteoclast progenitors. *Cancer Cell* **20**, 701–714 (2011).
- Asangani, I. A. *et al.* Therapeutic targeting of BET bromodomain proteins in castration-resistant prostate cancer. *Nature* **510**, 278–282 (2014).
- Maira, S.-M. *et al.* Identification and characterization of NVP-BE235, a new orally available dual phosphatidylinositol 3-kinase/mammalian target of rapamycin inhibitor with potent *in vivo* antitumor activity. *Mol. Cancer Ther.* **7**, 1851–1863 (2008).
- Nguyen, H. M. *et al.* Cabozantinib inhibits growth of androgen-sensitive and castration-resistant prostate cancer and affects bone remodeling. *PLoS ONE* **8**, e78881 (2013).
- Vitali, R. *et al.* Activity of tyrosine kinase inhibitor dasatinib in neuroblastoma cells *in vitro* and in orthotopic mouse model. *Int. J. Cancer* **125**, 2547–2555 (2009).
- Nair, A. B. & Jacob, S. A simple practice guide for dose conversion between animals and human. *J. Basic Clin. Pharm.* **7**, 27–31 (2016).
- Fazio, N. *et al.* A phase II study of BE235 in patients with everolimus-resistant, advanced pancreatic neuroendocrine tumours. *Anticancer Res.* **36**, 713–719 (2016).
- Carlo, M. I. *et al.* A phase Ib study of BE235, a dual inhibitor of phosphatidylinositol 3-kinase (PI3K) and mammalian target of rapamycin (mTOR), in patients with advanced renal cell carcinoma. *Oncologist* **21**, 787–788 (2016).
- Bjornson, Z. B., Nolan, G. P. & Fantl, W. J. Single-cell mass cytometry for analysis of immune system functional states. *Curr. Opin. Immunol.* **25**, 484–494 (2013).
- Yuen, A. K. L. & Hutton, C. A. Deprotection of pinacolyl boronate esters via hydrolysis of intermediate potassium trifluoroborates. *Tetrahedr. Lett.* **46**, 7899–7903 (2005).



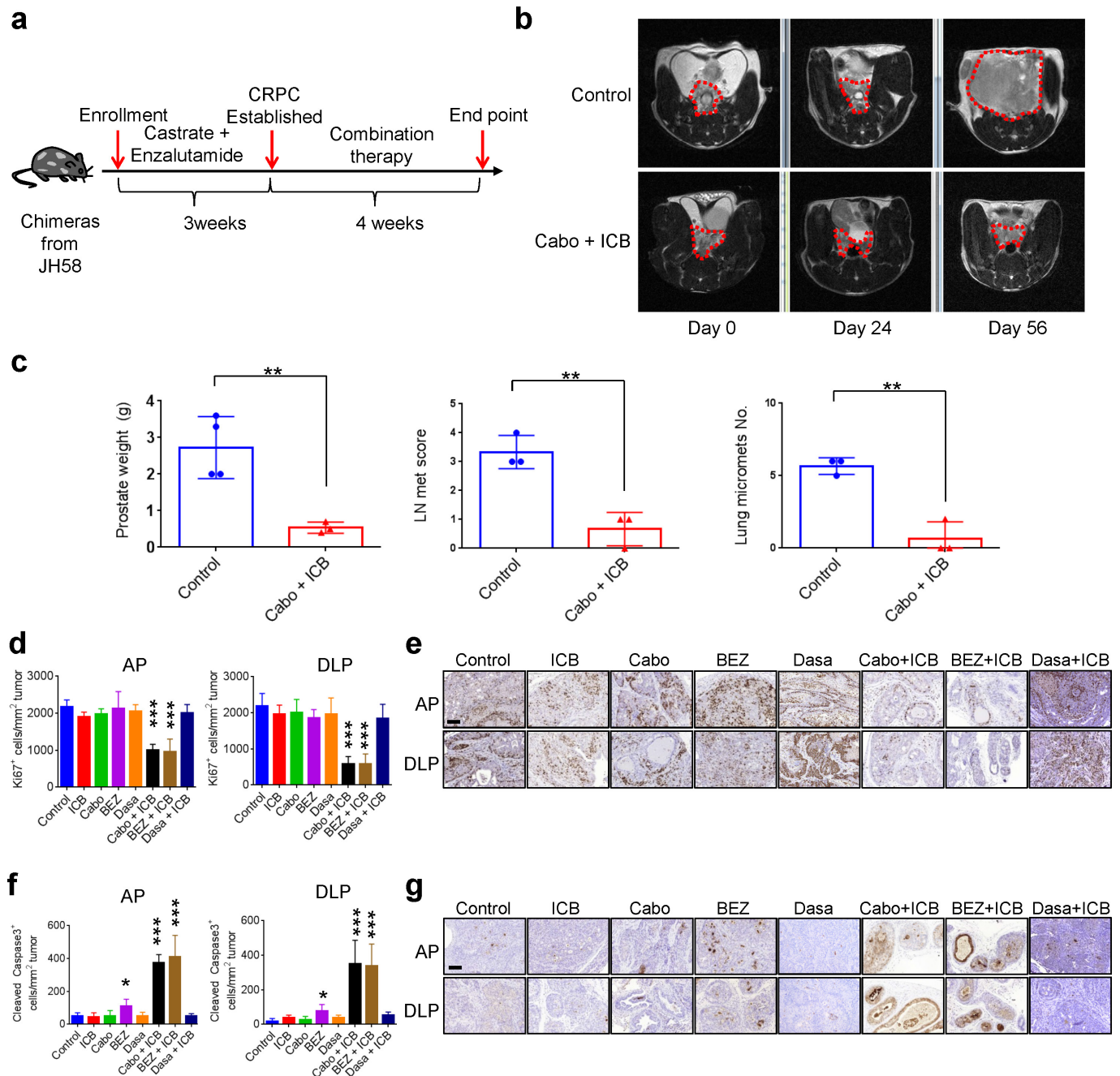
**Extended Data Figure 1 | Chimaeric modelling as an efficient approach to generating spontaneous metastatic PCa.** **a**, Comparison of probability of obtaining PCa-bearing males with CPPSML genotype in a litter, through breeding or chimaeric modelling. In chimaeric modelling, >75% coat colour contributed by injected mES cells (mESC in the figure) is defined as positivity for chimera. **b**, **c**, Predicted and experimental results for PCR-RFLP genotyping of the H2 locus from several mouse strains and two mES cell lines (JM8 is a standard mES cell line derived from C57BL/6 strain as control; Ep61 is also known as JH61). Red asterisk in **b** and yellow highlight wells in **c** indicate that the H2 haplotype for JH61 is H2<sup>b</sup>, the same as the C57BL/6 strain. **d**, SLP marker analysis of the region on chromosome 17 flanking the H2 complex locus (34–46 Mb), showing that JH61 has 100% C57BL/6 background in the H2 locus,

identical to the standard C57BL/6 mES cell line JM8. **e**, Experimental steps for generating the CPPSML chimaeras. **f**, Fluorescence images of prostate, draining lymph node (LN), and lung from a representative chimera at 3 months old. GFP<sup>+</sup> signals indicate the presence of metastasis to lymph nodes and disseminated tumour cells and micrometastasis in lung. Scale bars: prostate, 5 mm; lymph node and lung, 1 mm. **g**, Fluorescence microscopy and H&E image of snap-frozen prostate tumour from chimera showing that the GFP<sup>+</sup> area corresponds to adenocarcinoma and the GFP<sup>-</sup> area corresponds to normal host cells. Scale bar, 500 μm. **h**, Immunohistochemical staining showing the expansion of both CK8<sup>+</sup> luminal lineage and CK5<sup>+</sup> basal lineage in the prostate tumour formed in CPPSML chimera. Scale bar, 50 μm.



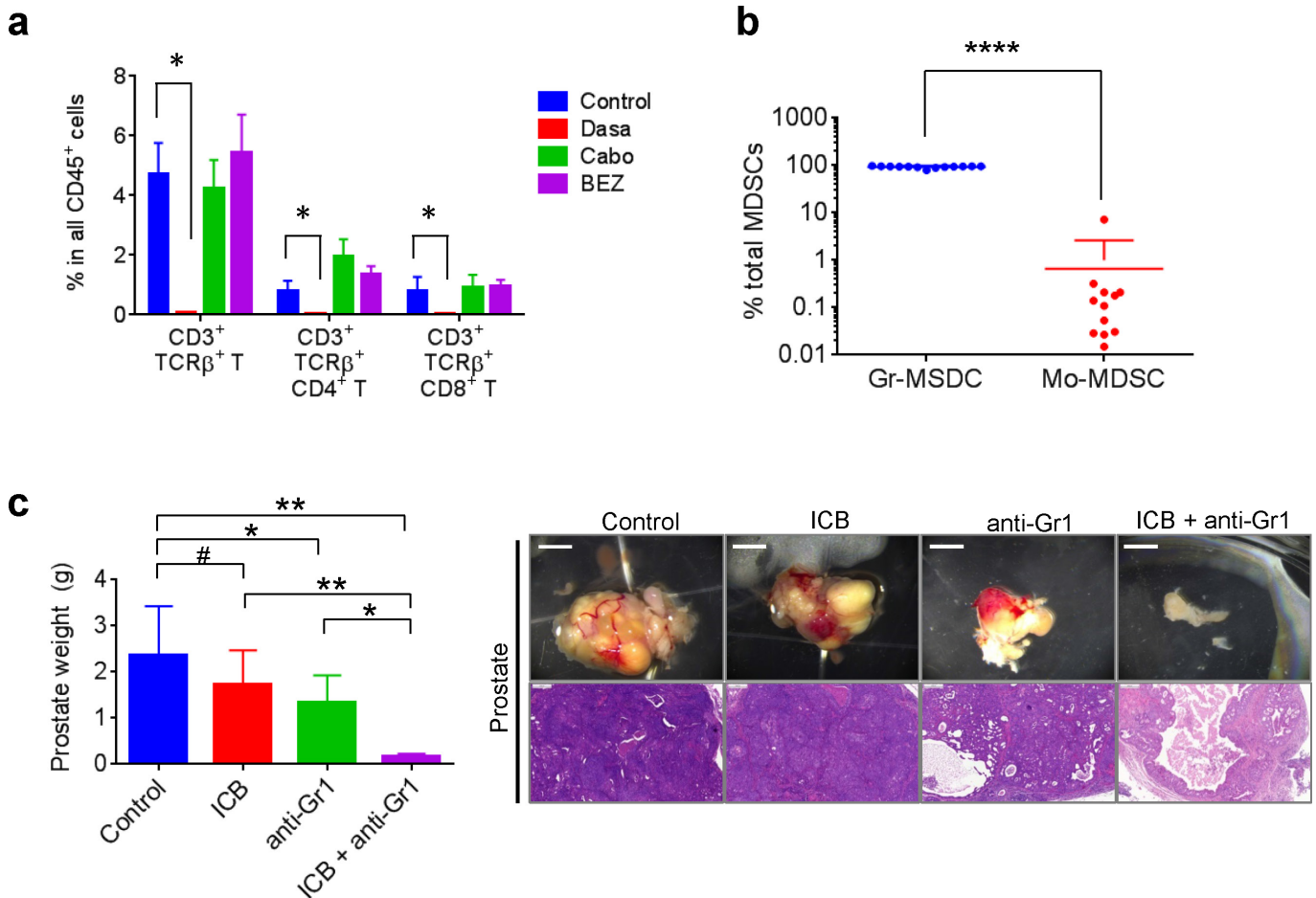
**Extended Data Figure 2 | Experimental design for preclinical therapy of mCRPC in CPPSML chimaeras.** **a**, Significant yet transient survival benefit by castration followed by diet admixed with enzalutamide (50 mg per kg diet) in *PB-Cre<sup>+</sup> Pten<sup>L/L</sup> p53<sup>L/L</sup> Smad4<sup>L/L</sup>* mice ( $n = 40$  and 18, respectively). \*\*\*\* $P < 0.0001$ , log-rank test. **b**, Record of assignment for drug trials showing the time range of prostate tumour formation in the CPPSML chimaera. **c**, Representative CPPSML chimaera with primary CRPC, lymph node metastasis, and micrometastasis in lung.

Scale bars: prostate, 5 mm; lymph node and lung, 1 mm. AP, DLP, and VP denote anterior, dorsolateral, and ventral prostate lobes, respectively. **d**, Experimental flow for creating mCRPC cohorts and preclinical testing of monotherapy and combination therapy, followed by tumour characterization. **e**, Representative images of prostate tumours with H&E staining, and GFP<sup>+</sup> tumour cells in the lymph node and lung. Scale bars: prostate, 5 mm; lymph node and lung, 1 mm; H&E, 200  $\mu$ m.



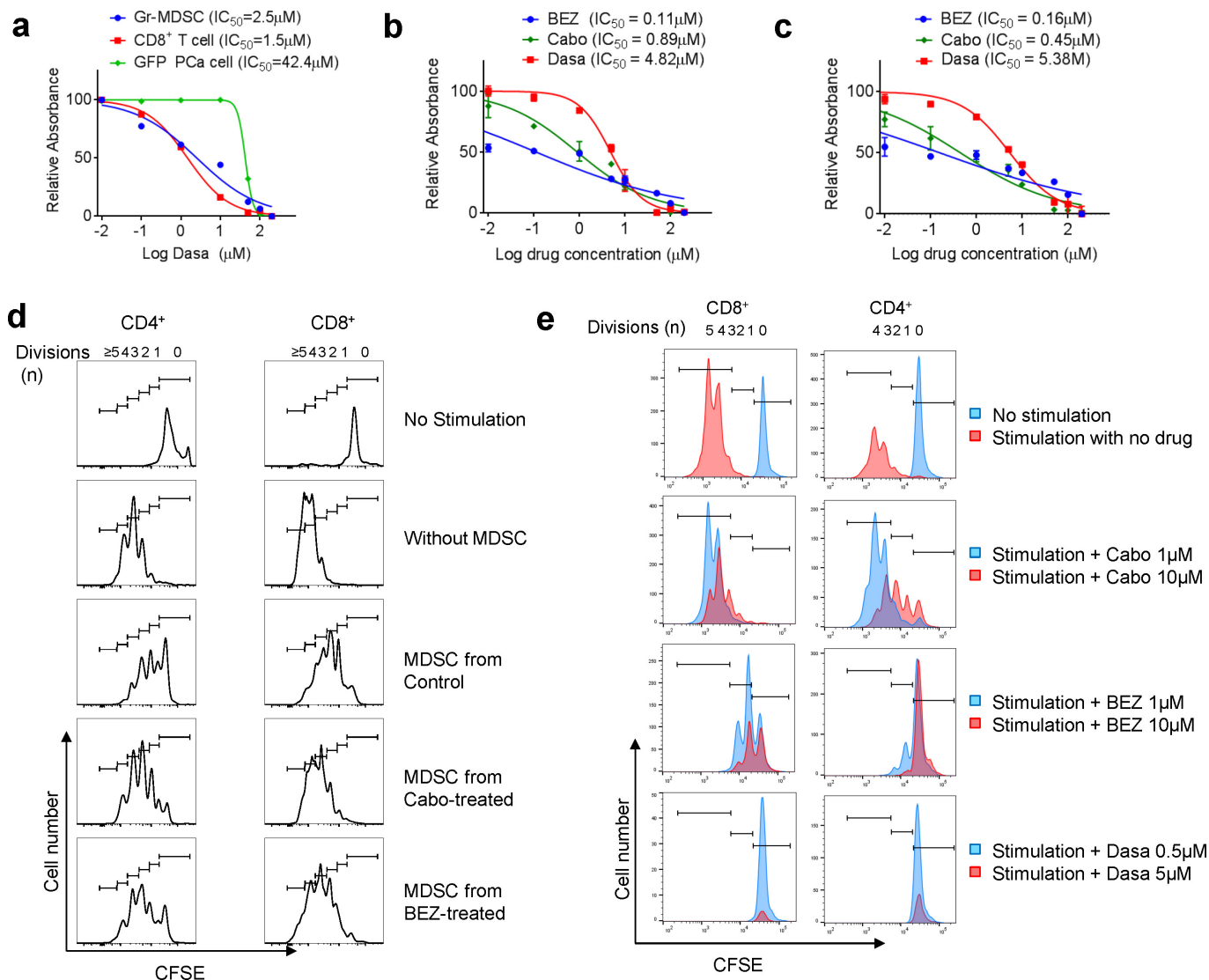
**Extended Data Figure 3 | Significant combination efficacy by cabozantinib and ICB observed in chimaeras generated from JH58.**  
**a**, Experimental design for JH58 chimaeras, similar to the JH61 chimaera experiments. **b**, Longitudinal MRI images from representative chimaeras in control or combination cohorts. Red contour denotes area of prostate tumour. **c**, Strong anti-tumour effect by combination therapy in JH58 chimaeras shown by prostate tumour mass, lymph node metastasis scores and lung micrometastasis number ( $n = 3$ , biological replicates).

$**P < 0.01$ , Student's  $t$ -test. **d, e**, Quantification of tumour cell proliferation by Ki67 immunohistochemistry ( $n = 4$ , biological replicates) with representative images. Anterior prostate (AP) and dorsolateral prostate (DLP) were quantified separately. **f, g**, Quantification of tumour cell apoptosis by cleaved caspase 3 immunohistochemistry ( $n = 5$ , biological replicates) with representative images. Scale bar,  $100 \mu\text{m}$ . In **c, d**, and **f**, data represent mean  $\pm$  s.d.  $*P < 0.05$ ,  $**P < 0.01$ ,  $***P < 0.001$ , compared with control using Student's  $t$ -test.



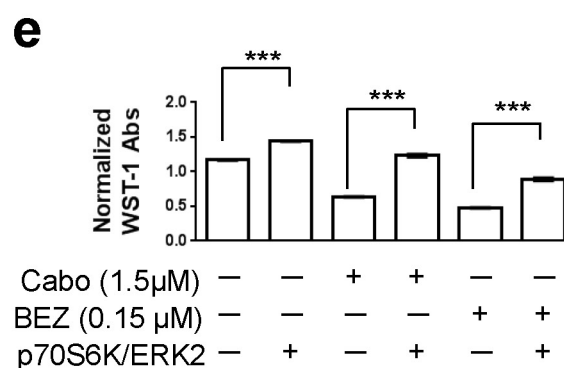
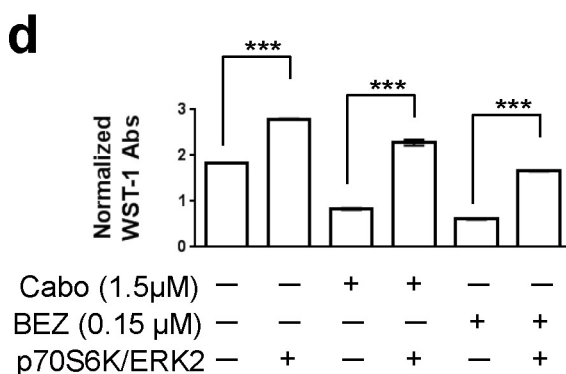
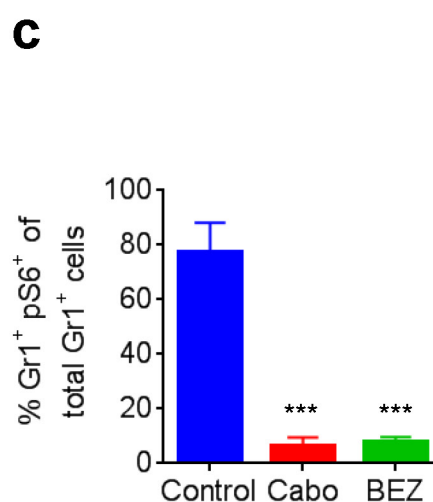
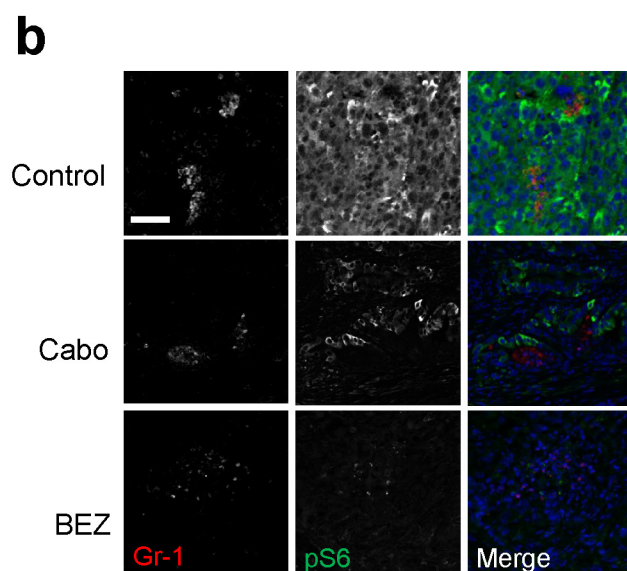
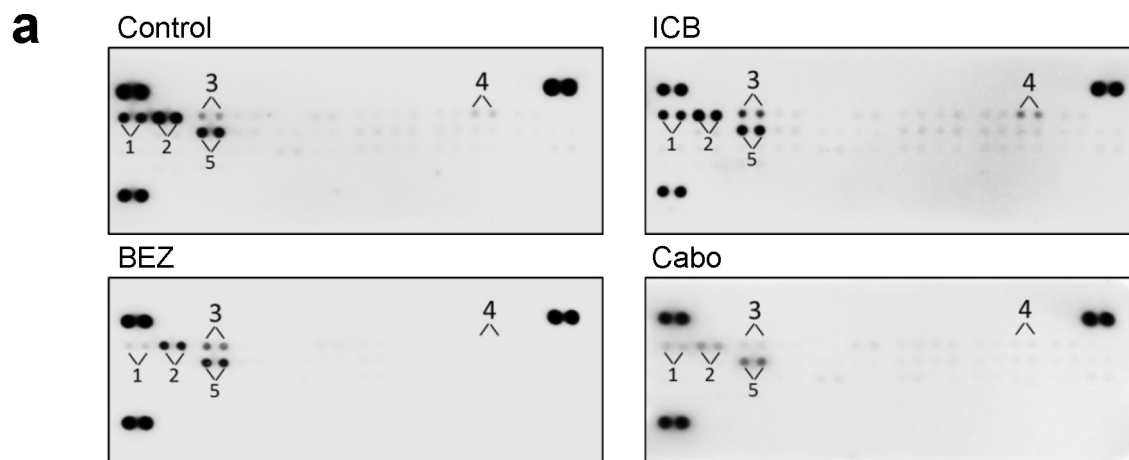
**Extended Data Figure 4 | Combination efficacy by Gr1 neutralizing antibody with ICB.** **a**, Dasatinib, but not cabozantinib or BEZ235, significantly reduced the frequency of infiltrating T cells in CRPC of CPPSML mice ( $n = 4$ , biological replicates). Data represent mean  $\pm$  s.e.m.  $*P < 0.05$ , Mann-Whitney  $U$ -test. **b**, Frequency of Gr-MDSCs and Mo-MDSCs in CPPSML prostate tumours ( $n = 13$ , biological replicates). **c**, Mass and representative whole-organ and H&E images of prostate

tumours from CPPSML chimaeras induced to develop CRPC and treated with 1 month of control IgG, ICB (anti-CTLA4 plus anti-PD1 antibodies), anti-Gr1 neutralizing antibody, or combination of ICB and anti-Gr1 ( $n = 4$ , biological replicates). Scale bars: 3 mm for organ images, 200  $\mu$ m for H&E images. In **b** and **c**, data represent mean  $\pm$  s.d.  $*P < 0.05$ ,  $**P < 0.01$ ,  $****P < 0.0001$ ,  $\#P > 0.05$ , Mann-Whitney  $U$ -test.



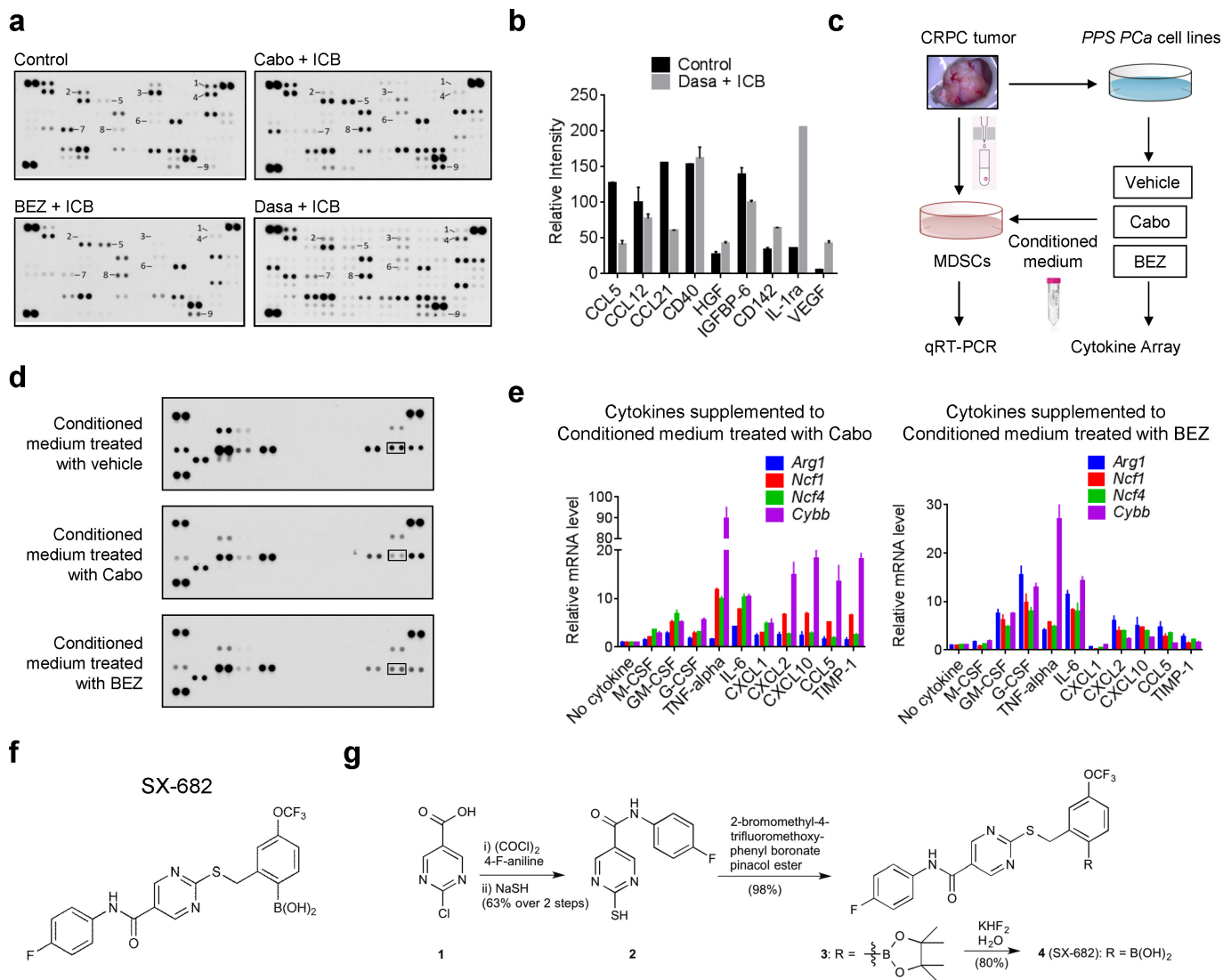
**Extended Data Figure 5 | Characterization of the effect of drugs on MDSCs.** **a**, Comparison of *in vitro* sensitivity to Dasa by MDSCs, CD8<sup>+</sup> T cells, and GFP<sup>+</sup> cancer cells isolated from CRPC of CPPSML mice. Cell viability was measured 24 h after the start of drug treatment using the WST-1 assay.  $IC_{50}$  values are indicated. **b**, Comparison of *in vitro* sensitivity to BEZ, Cabo, and Dasa by MDSCs isolated from CRPC of CPPSML mice. The assay was performed in RPMI1640 supplemented with 10% FBS and 10 ng ml<sup>-1</sup> GM-CSF ( $n = 2$ , biological replicates). **c**, Comparison of *in vitro* sensitivity to BEZ, Cabo, and Dasa by MDSCs

isolated from CRPC of CPPSML mice. The assay was performed in RPMI1640 supplemented with 10% FBS, 10 ng ml<sup>-1</sup> GM-CSF, and pre-conditioned for 12 h by PCa cell lines established from the CPPSML model ( $n = 2$ , biological replicates). **d**, Representative CFSE flow cytometry histograms showing the effect on *in vitro* T-cell proliferation by MDSCs isolated from CRPC of CPPSML mice treated with the indicated drugs. Position of CFSE peaks can be used to denote the T-cell division times. **e**, Representative CFSE flow cytometry histograms showing the effect of Cabo, BEZ, and Dasa on *in vitro* T-cell proliferation.



**Extended Data Figure 6 | Cabozantinib and BEZ235 inhibit PI3K signalling in prostate tumour and intratumoural MDSCs.** **a**, Mouse phospho-RTK array measuring phospho-RTK activity in prostate tumours with indicated treatments. Numerals 1–5 represent pEGFR, pErbB2, pErbB3, pAxl, and pPDGFR $\alpha$ , respectively ( $n=2$ , biological replicates). **b**, **c**, Reduced pS6 signal in intratumoural MDSCs by Cabo and BEZ treatment, revealed by immunofluorescent co-staining of pS6 and Gr-1 ( $n=3$ , biological replicates). Scale bar, 100  $\mu\text{m}$ . **d**, WST-1 assay showing that co-transfection of active ERK2 and p70S6K proteins mediated the

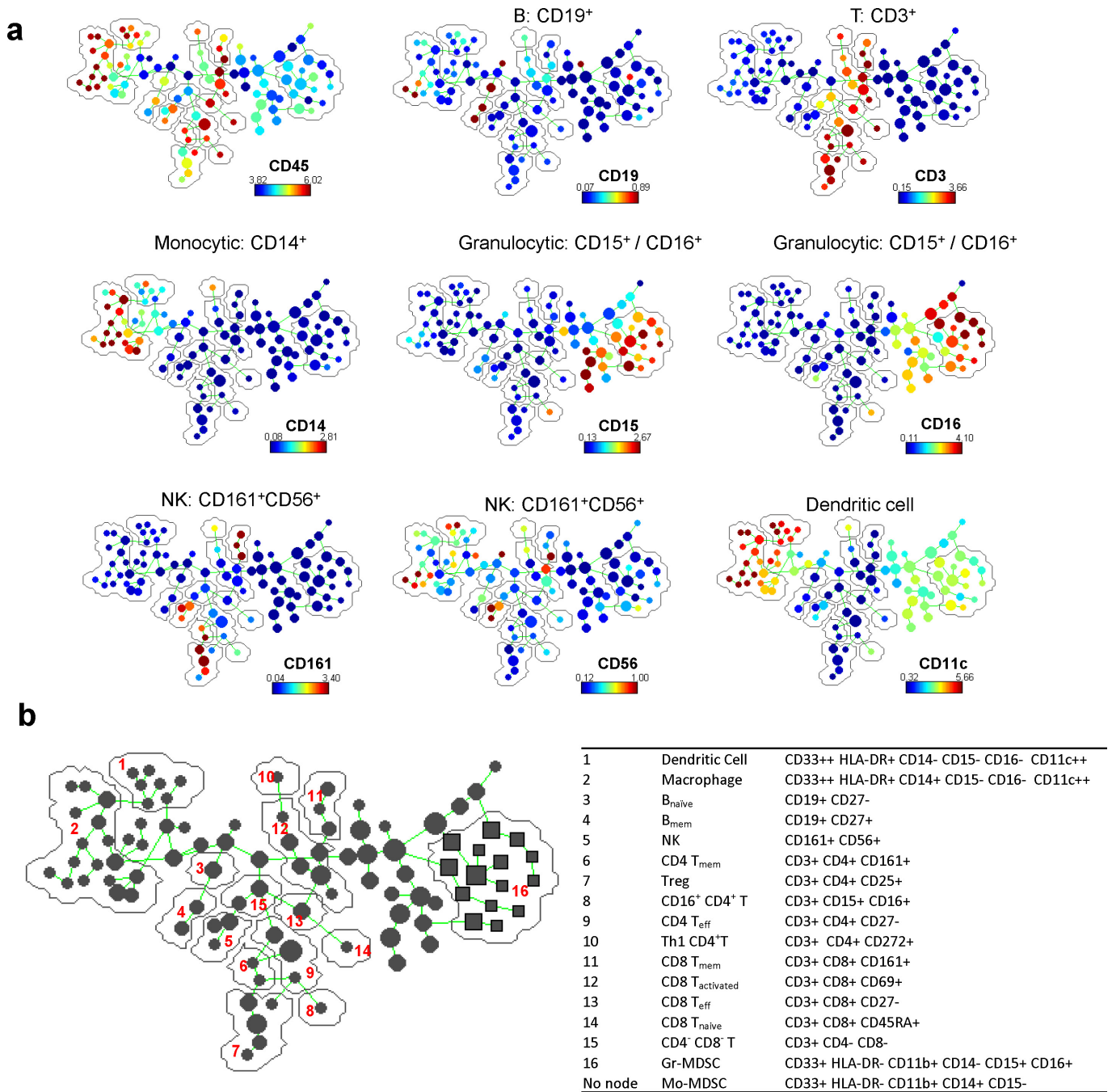
resistance of MDSCs isolated from CPPSML tumours to the cytotoxicity by Cabo (1.5  $\mu\text{M}$ ) or BEZ (0.15  $\mu\text{M}$ ). The assay was performed in RPMI1640 supplemented with 10% FBS and 10  $\text{ng ml}^{-1}$  GM-CSF ( $n=3$ , biological replicates). **e**, WST-1 assay similar to **d**, but performed in RPMI1640 supplemented with 10% FBS, 10  $\text{ng ml}^{-1}$  GM-CSF, and pre-conditioned for 12 h by Pca cell lines established from the CPPSML model ( $n=3$ , biological replicates). In **c–e**, data represent mean  $\pm$  s.d. \*\*\* $P < 0.001$ , Student's  $t$ -test.



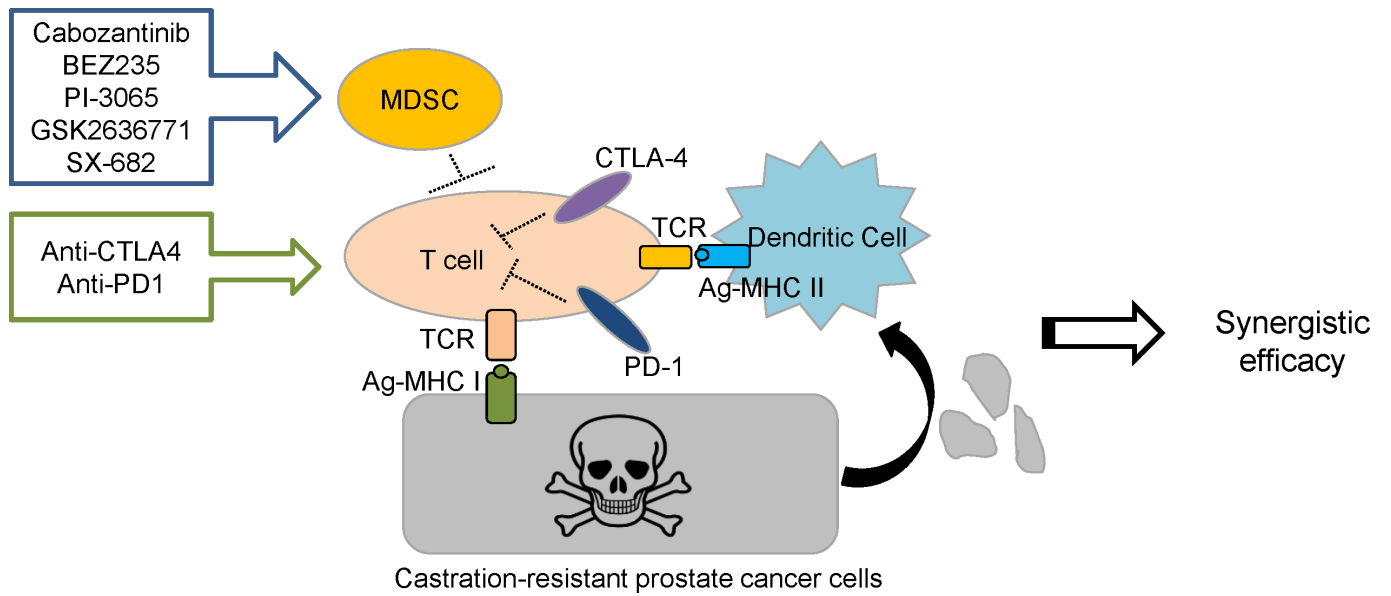
### Extended Data Figure 7 | Cabozantinib or BEZ235 suppress secretion by PCa cells of several cytokines that promote MDSC activity.

**a**, Quantification of intratumoural cytokine levels in CRPC chimaera tumours with indicated treatment using cytokine array ( $n = 2$ , biological replicates). Numerals 1–9 represent CCL5, CCL12, CCL21, CD40, CD142, HGF, IGFBP-6, IL-1ra, and VEGF, respectively. **b**, Quantification of intratumoural cytokine levels in Dasa + ICB combination-treated CPPSML chimaera CRPC with mouse cytokine assay, with image and relative intensity of the numbered cytokines shown ( $n = 2$ , biological replicates). **c**, Experimental design for MDSC culture in the presence

of PCa conditioned medium. **d**, Cytokine array results for conditioned medium from CPPSML PCa cell lines treated with vehicle, Cabo (1  $\mu$ M), or BEZ (1  $\mu$ M) for 12 h ( $n = 2$ , biological replicates). Boxed cytokine is CCL5. **e**, Effect of supplementation of individual cytokines to the conditioned medium from PCa cell lines treated with Cabo (1  $\mu$ M) or BEZ (1  $\mu$ M) on *Arg1*, *Cybb*, *Ncf1*, and *Ncf4* from cultured MDSCs ( $n = 3$ , biological replicates). **f**, **g**, Chemical structure and synthesis of allosteric CXCR1/2 antagonist SX-682 (Syntrix Biosystems). For details, please refer to the corresponding section in Methods. In **b**, **e**, and **f**, data represent mean  $\pm$  s.d.



**Extended Data Figure 8 | Detailed cell population annotation in SPADE tree.** a, SPADE tree coloured by the median intensity of individual markers (indicated above colour bar) to facilitate the assignment of tree branches to individual cell populations (shown on the top of each plot) ( $n = 12$ , biological replicates). b, Surface markers of different immune subpopulations representing small branches of the SPADE tree.



**Extended Data Figure 9 | Model depicting the combination therapy strategy in treating mCRPC.** As demonstrated in the CPPSML chimaera model, targeted therapy with agents that inhibit MDSC infiltration frequency and immunosuppressive activity can synergize with ICB to invigorate T-cell immunity in the prostate tumour microenvironment and thus impair CRPC progression.

Extended Data Table 1 | Additional information on mouse model, clinical samples, and methodology

a

JH61 chimeras	# chimera	Percent
90-100%	56	48.7
75-90%	35	30.4
50-75%	14	12.2
under 50%	10	8.7
TOTAL	115	100

b

Marker	Clone	Label	Vendor	Cat#
CD19	H1B19	142Nd	DVS-Sunnyvale	3142001B
CD357, GITR	621	143Nd	BioLegend	311602
CD11b	ICRF44	144Nd	DVS-Sunnyvale	3144001B
CD4	RPA-T4	145Nd	DVS-Sunnyvale	3145001B
CD8a	RPA-T8	146Nd	DVS-Sunnyvale	3146001B
CD278, ICOS	C398.4A	147Sm	BioLegend	313502
CD134, OX40	Ber-ACT35	148Nd	BioLegend	350002
CD223, LAG-3	Poly	149Sm	R&D	AF2319
CD202b(Tie2/Tek)	33.1(Ab33)	150Nd	BioLegend	334202
CD123	6H6	151Eu	DVS-Sunnyvale	3151001B
CD137	4-1BB	152Sm	BD	555955
CD133/2	293C3	153Eu	Miltenyi	130-090-851
CD45	HI30	154Sm	DVS-Sunnyvale	3154001B
TIM-3	F38-2E2	156Gd	BioLegend	345002
CD33	WM53	158Gd	DVS-Sunnyvale	3158001B
CD11c	Bu15	159Tb	DVS-Sunnyvale	3159001B
CD161	191B8	161Dy	Miltenyi	191B8 custom
CD69	FN50	162Dy	DVS-Sunnyvale	3162001B
CD45RA	HI100	163Dy	BioLegend	304102
CD15	W6D3	164Dy	DVS-Sunnyvale	3164001B
CD16	3G8	165Ho	DVS-Sunnyvale	3165001B
CD44	BJ18	166Er	DVS-Sunnyvale	3166001B
CD27	O323	167Er	DVS-Sunnyvale	3167002B
CD38	HIT2	168Er	BioLegend	303502
CD25	2A3	169Tm	DVS-Sunnyvale	3169003B
CD3	UCHT1	170Er	DVS-Sunnyvale	3170001B
CD62L	DREG-56	171Yb	BioLegend	304802
CD274, PD-L1	29E.2A3	172Yb	BioLegend	329702
CD14	HCD14	173Yb	BioLegend	325602
HLA-DR	L243	174Yb	DVS-Sunnyvale	3174001B
CD279, PD-1	J105	175Lu	MBL	D133-3
CD56	HCD56	176Yb	DVS-Sunnyvale	3176001B

c

Patient ID	Gleason Score (Grades)	pStage	pN Stage	Race
880709	9(4+5)	pT3b	N0	H
880503	7(3+4)	pT2	N0	W
882696	7(3+4)	pT2	N0	W
883678	7(4+3)	pT2	N0	W
883121	7(4+3)	pT3a	N0	W
882002	9(4+5)	pT3b	N1	W
883318	9(4+5)	pT3b	N0	W
885177	7(4+3)	pT2	N0	A
885567	7(3+4)	pT2	N0	W
885592	7(4+3)	pT2	N0	W

a, Coat colour chimaerism for chimaeras derived from JH61. b, CyTOF antibody panel for human prostate tumour samples. c, Clinical information of the fresh fine-needle biopsy specimens.